CHALMERS
UNIVERSITY OF TECHNOLOGY

Wave transmission analysis of marine structures

Evaluating the accuracy of different theoretical models for determining the transmission coefficient

Master's thesis in Naval Architecture and Ocean Engineering

Jonathan Lundström

DEPARTMENT OF MECHANICS AND MARITIME SCIENCES
DIVISION OF MARINE TECHNOLOGY

CHALMERS UNIVERSITY OF TECHNOLOGY
Gothenburg, Sweden 2021
www.chalmers.se

MASTER'S THESIS IN NAVAL ARCHITECTURE AND OCEAN ENGINEERING

Wave transmission analysis of marine structures

Evaluating the accuracy of theoretical models for determining the transmission coefficient

Jonathan Lundström

Department of Mechanics and Maritime Sciences
Division of Marine Technology
CHALMERS UNIVERSITY OF TECHNOLOGY
Göteborg, Sweden 2021

Wave transmission analysis of marine structures
Evaluating the accuracy of theoretical models for determining the transmission coefficient
Jonathan Lundström

Master's Thesis 2021:13
Department of Mechanics and Maritime Sciences
Division of Marine Technology
Chalmers University of Technology
SE-412 96 Göteborg
Sweden
Telephone: + 46 (0)31-772 1000

Cover:
Rendering of a SFBW1000(3.0) breakwater by SF Marina

Chalmers University of Technology / Department of Mechanics and Maritime Sciences
Göteborg, Sweden 2021-06-04

Wave transmission analysis of marine structures
Evaluating the accuracy of theoretical models for determining the transmission coefficient
Master's thesis in Naval Architecture and Ocean Engineering
Jonathan Lundström
Department of Mechanics and Maritime Sciences
Division of Marine Technology
Chalmers University of Technology

Abstract

Analyzing the performance of floating breakwaters is no easy task and there are many different theoretical models, developed to do this. The different theoretical models vary in complexity and are derived for different types of breakwaters. To find the best suiting theoretical model, measurements of the incoming and transmitted wave climate are conducted. In total, 11 different theoretical models and one software, Ansys AQWA, are compared with the measured data. To compare the result from the theoretical models and software with the measured data, the measured data is filtered and averaged over time. The results show that two of the theoretical models correlate well with measured data. The wave measurement data also shows that the breakwater performance is dependent on the incoming wave climate and that the incoming wave climate is dependent on the wind climate. In the study, an IMU sensor is used to measure the movement of the breakwater. By comparing the IMU data with the wave data it is seen that the movement of the breakwater depends on the incoming wave climate. More measurements are needed to evaluate if the movement of the breakwater affects the transmission performance of the breakwater.

Keywords: Wave transmission, Marine structures, Breakwater performance, Transmission models, Transmission coefficient, Wave climate

Contents

Preface

In this study, the wave climate around a floating breakwater and the breakwater movement have been measured. Different theoretical models for estimating breakwater performance have been studied and compared with the measured wave climate. The wave measurements were carried out during three periods, the first between the 20th of November 2020 until the 5th of January 2021, the second was between the 29th of January 2021 until the 15th of March 2021, and the third was conducted between the 18th of March 2021 until the 5th of May 2021. The study was carried out as a master´s thesis in Naval Architecture and Ocean Engineering at the Department of Mechanics and Maritime Sciences and the division of Marine technology at Chalmers University of Technology, together with SF Marina System AB.

The master's thesis has been carried out with Professor Carl-Erik Janson as a supervisor and Senior Lecturer Per Hogström as the examiner. I would like to thank them both for their help and support throughout the study. I would also like to thank Lina Odhe, Michael Sigvardson, Jasmine Person, and all other personnel at SF Marina System AB for the opportunity to carry out this study and for their help and support throughout the project. Lastly, I would like to thank Helmer Palmgren and Karolina Beskow at Sweco and the staff at the Chalmers Library for helping me track down sources for the different theoretical models.

Göteborg March 2021-06-04

Jonathan Lundström

Notations

Roman upper case letters

B	Breakwater breadth [m]
B_e	Effective breadth of breakwater [m]
C	Wave celerity [m/s]
D	Breakwater draft [m]
E	Total energy [J/m^2]
F	Fetch [m]
H	Wave height [m]
H_c	Unknown coefficient in Weibull distribution
H_i	Wave height of incoming wave [m]
H_m	Metacentric height [m]
H_{max}	Maximum wave height [m]
H_s	Significant wave height [m]
H_t	Wave height of transmitted wave [m]
I_m	Moment of inertia [$kg\ m^2$]
L	Wavelength [m]
M	Width of running mean filter
M_{GK}	Constant from Günaydin and Kebdaşli (2007)
N	Number of waves in the sample
N_{GK}	Constant from Günaydin and Kebdaşli (2007)
$N_{samples}$	Number of measurements in one wave burst
$N_{spectral}$	Number of spectral points in wave burst measurement
P	Breakwater mass [N]
P_i	Probability [$\%$]
Par_1	Non-dimensional variable from Günaydin and Kebdaşli (2007)
S	Spectral variance density
T	Wave period [s]
T_1	Mean wave period [s]
$T_{1/3}$	Significant wave period [s]
T_n	Natural period [s]
T_p	Peak period [s]
T_{Sample}	Sample time [s]

T_z	Mean zero up-crossing period [s]
U	Wind speed [*m/s*]

Roman lower case letters

a_i	Accelerometer output in direction *i* [g]
c_t	Wave transmission coefficient
d	Water depth [m]
$\bar{d}$	Mean water depth [m]
f	Measurement frequency [*Hz*]
f_{res}	Frequency resolution [*Hz*]
g	Gravitational acceleration, $\left[\frac{m}{s^2}\right]$
g_i	Gyroscope output in direction *i* [*dps*]
k	Wavenumber [*rad/m*]
$m_0^{1/2}$	Standard deviation of surface elevation
m_i	Magnetometer output in direction *i* [°]
m_n	nth spectral moment
n_j	Cumulated sum of occurrences
y_0	Non-dimensional coefficient used by Hunt (1979)

Other symbols

α	Angle between the wave crest and breakwater wall [°]
$\beta(\chi)$	Correction equation from Ruol et al. (2013)
χ	Scaling parameter from Ruol et al. (2013)
χ_0	Constant from Ruol et al. (2013)
ϕ	Roll angle [°]
$\bar{\phi}$	Filtered roll angle [°]
γ	Unknown coefficient in Weibull distribution
ω	Wave frequency [*rad/s*]
ρ	Fluid density [kg/m^3]
σ	Constant from Ruol et al. (2013)
θ	Pitch angle [°]
$\bar{\theta}$	Filtered pitch angle [°]
ψ	Yaw angle [°]
$\bar{\psi}$	Filtered yaw angle [°]

1 Introduction

This study evaluates methods of estimating the performance of floating breakwaters and in the introduction, some basic information regarding the study is presented. This section presents the background to the study as well as the purpose and limitations. The properties used to estimate the performance are presented for the breakwater that will be studied.

1.1 Background

To understand the problem at hand, some background information is needed. First, the wave climate in harbors is discussed to get an understanding of what is considered a "good" wave climate. Different types of breakwaters and anchoring systems are presented and briefly compared before discussing how the performance of breakwaters is evaluated.

1.1.1 Wave climate in harbors

In marinas all over the world, breakwaters are used to create a safe wave environment for the vessels located within the marina. A safe wave environment is defined differently by different standards.

Table 1.1 presents the recommended wave height for different wave periods and wave directions (Institution of civil engineers 1992). The values in Table 1.1 do not take into account that the effect of the waves on the vessels is dependent on the size of the vessel. In 1995 the MarCom working group at PIANC developed a new criterion, presented in Table 1.2, where the size of the vessel also is considered. (MarCom Working Group 1995)

1.1.2 Fixed and floating breakwaters

Two types of breakwaters are used, floating breakwaters, and fixed breakwaters. Fixed breakwaters are rigid structures that are built on the seabed and protect the marina by diverting all incoming waves. Due to that they extend from the bottom to the surface, the wave energy is not able to transmit through the breakwater and hence all incoming waves will be reflected away from the breakwater.

Floating breakwaters are floating structures that can move with the waves and are held in place with an anchoring system. There are many different types of floating breakwaters and the different types have different advantages and disadvantages. McCartney (1985) divides the floating breakwaters into 4 different categories and discusses the features and performance of the different floating breakwaters. However, all types of floating breakwaters have a common disadvantage. They do not extend from the bottom to the surface and thus, some of the incoming waves will be transmitted through the breakwater.

Table 1.1 Wave climate criteria from the Canadian Department of Fisheries and Oceans (Institution of civil engineers 1992)

Provisionally Recommended Criteria for A "Good" wave Climate in Small Craft Harbours			
Direction and peak period of design harbor wave	Wave event exceeded once in 50 years	Wave event exceeded once a year	Wave event exceeded once each week
Head seas less than 2 seconds	Not likely to occur during this event	Wave height less than 0.30m	Wave height less than 0.30m
Head seas between 2 and 6 seconds	Wave height less than 0.60m	Wave height less than 0.30m	Wave height less than 0.15m
Head seas greater than 6 seconds	Wave height less than 0.60m or 1.20m horizontal wave motion	Wave height less than 0.30m or 0.60m horizontal wave motion	Wave height less than 0.15m or 0.46m horizontal wave motion
Oblique seas	Less than $0.3048 \cdot (2 - 1.25\sin(\theta))$m where θ is the angle from the head sea	Less than $0.3048 \cdot (1 - 0.5\sin(\theta))$m where θ is the angle from the head sea	Less than $0.3048 \cdot (0.5 - 0.25\sin(\theta))$m where θ is the angle from the head sea
Beam seas less than 2 seconds	The condition is not likely to occur during this event	Wave height less than 0.30m	Wave height less than 0.30m
Beam seas between 2 and 6 seconds	Wave height less than 0.23m	Wave height less than 0.15m	Wave height less than 0.08m
Beam seas greater than 6 seconds	Wave height less than 0.23m or 0.60m horizontal wave motion	Wave height less than 0.15m or 0.30m horizontal wave motion	Wave height less than 0.08m or 0.23m horizontal wave motion
For criteria for an "excellent" wave climate multiply by 0.75 and for a moderate wave climate multiply with 1.25			

Table 1.2 Wave climate criteria for different Vessel sizes (MarCom Working Group 1995)

Wave event exceeded once a year				
Vessel length [m]	Beam/Quartering seas		Head seas	
	Wave period [s]	Wave height [m]	Wave period [s]	Wave height [m]
4.0 – 10.1	< 2.0	0.21	< 2.5	0.21
	2.0 – 4.0	0.09	2.5 – 4.0	0.15
	> 4.0	0.15	> 4.0	0.21
10.1 – 15.8	< 3.0	0.24	< 3.5	0.30
	3.0 – 5.0	0.15	3.5 – 5.5	0.21
	> 5.0	0.21	> 5.5	0.30
20.1	< 4.0	0.30	< 4.5	0.30
	4.0 – 6.0	0.15	4.5 – 7.0	0.24
	> 6.0	0.24	> 7.0	0.30

The disadvantages of the floating breakwater are however compensated with other benefits. McCartney (1985) states that some of the advantages of using floating breakwaters instead of fixed breakwaters are:

- Possibility to have breakwaters at locations with poor seabed foundations that do not support fixed breakwaters.
- Possibility to have breakwaters where the water depth is too large for fixed breakwaters.
- Less interference with water circulation and fish migration.
- Possibility to move the breakwaters to a protected area during ice formation.
- Lower freeboard, since the floating breakwaters move with the tide.
- Possibility to rearrange the floating breakwaters to fit future needs.

The floating breakwaters are considered to have a smaller footprint than the fixed breakwaters due to that the floating breakwaters are only attached to the seabed through the anchoring system. This can be seen when comparing Figure 1.1 with Figure 1.2 where two different types of floating and fixed breakwaters are visualized. In addition, Dai et al. (2018) state that the fixed breakwaters impede water circulation which in turn leads to increased pollution and sediment issues on the protected side of the breakwater. From an environmental point of view, floating breakwaters are thus preferred.

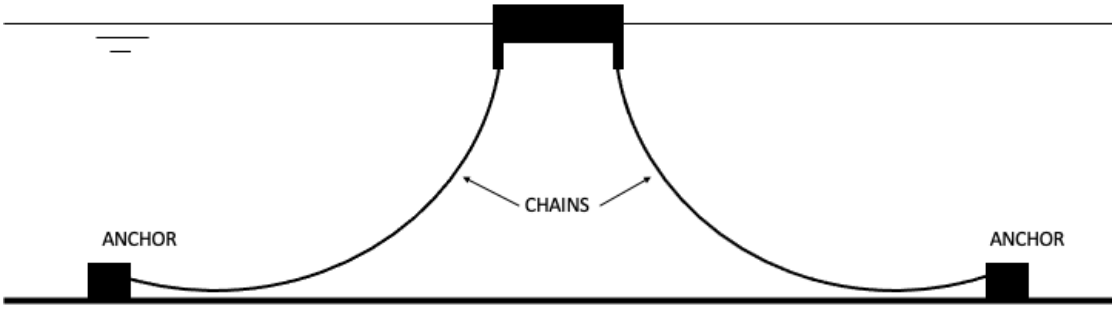

Figure 1.1 Floating breakwater, moored with chains and anchors.

Figure 1.2 Rubble mound fixed breakwater.

1.1.3 Anchoring systems of floating breakwaters

There are many different types of anchoring systems that can be used for floating breakwaters. According to McCartney (1985), the three most common anchoring systems are piling, anchors, and stake piles. The different anchoring systems have different limitations and affect wave dampening in different ways.

The piling method uses large piles that are sunken into the seabed and then connected to the floating breakwaters. Piling allows the breakwaters to move in the vertical direction but restricts movement in the horizontal plane. Anchors and stake piles are positioned on the seabed and then connected to the breakwater using either chains or lines. These allow the breakwater to move in all directions but restrict the magnitude of the movement. If chains are used, they will also help to dampen the movements due to their weight. (McCartney 1985)

According to Cox and Beach (2006), breakwaters using piling are preferred in Australia due to that the anchor and stake pile anchoring systems require high inspection and maintenance costs. However, in some cases where the bottom is not suitable for piles or the water depth is too great, anchors or stake piles might be the only option. (McCartney 1985)

1.1.4 Performance of floating breakwaters

When an incoming wave reaches a floating breakwater the energy within the wave is divided into three parts. One part continues through the breakwater, this part is known as the transmitted wave. The second part is reflected by the breakwater and creates a new reflected wave. The last part of the energy dissipates, either in the form of turbulence in the water surrounding the breakwater, or friction in connections between breakwaters. (Peña González et al., 2011)

When evaluating the performance of a floating breakwater it is common to look at the wave transmission coefficient. The wave transmission coefficient is defined as the height of the transferred wave over the height of the incoming wave as shown in Equation 1.1 (Cox and Beach 2006). A high value of the transmission coefficient correlates to a bad performance of the breakwater since most waves are transmitted through the breakwater.

$$c_t = \frac{H_t}{H_i} \tag{1.1}$$

1.2 Purpose

This study will analyze a floating breakwater from SF MARINA, a Swedish company that designs and builds floating breakwaters and pontoons for marinas all over the world. Their design is developed through theory and many years of experience. Many different theoretical models exist that could be used for estimating the breakwater performance. It is unknown how well these models fit the breakwaters from SF MARINA. (L. Odhe, personal communication, September 23, 2020).

The purpose of the study is divided into three parts. The first purpose is to evaluate the performance of the floating breakwater located in Skärhamn. The second purpose is to compare the measured performance with existing estimation methods to find the most accurate method to estimate the performance of floating breakwaters. The last purpose of the study is to analyse how the movement of the breakwater correlates with the wave transmission. The results from this study might be possible to use to develop a new method for estimating the performance of the floating breakwaters from SF MARINA.

1.3 Limitations

The study is carried out on a SFBW1000(3.0) breakwater from SF MARINA located in Skärhamn, Sweden. All calculations will be carried out with values from this specific breakwater and location. The breakwater will be considered as a rigid body with six degrees of freedom to simplify calculations.

It is not the purpose of this study to evaluate the difference between floating and bottom-connected breakwaters. The study will only focus on the floating Π-shaped breakwater and no comparison of performance between different types of floating breakwaters will be carried out. It is also not the purpose of this study to evaluate how different anchoring systems affect the performance of the breakwater. The breakwater that will be studied is moored using chains and concrete anchors.

The study will not evaluate the ecological, economic nor societal impact of floating breakwaters since the objective of the study is simply to evaluate the performance of an existing breakwater. It is not the objective of this study to optimize the design of breakwaters since the theoretical model will be optimized for this specific design.

1.4 Breakwater properties

In Skärhamn, the breakwater consists of four sections of SFBW1000(3.0) connected in series, and anchored using chains and anchors. The different sections vary slightly but the main parameters are the same for all breakwaters. The parameters are presented in Table 1.3 and all values are obtained directly from SF MARINA.

Table 1.3 Breakwater properties

Properties	Value	Unit
Length	20	m
Breadth	10	m
Height	3	m
Draft	2.2	m
Mass	195 - 200	$tons$
KG	2.09	m
Ixx	$1.95 \cdot 10^6$	$kg\ m^2$
Iyy	$6.46 \cdot 10^6$	$kg\ m^2$
Izz	$8.15 \cdot 10^6$	$kg\ m^2$

2 Theory

The theory section presents some basics in wave theory and the theory behind the different theoretical models that will be evaluated later on in this report. Equations for different wave properties such as wavenumber, angular frequency, wave celerity, and wavelength are presented as well as some theories behind breakwater motion analysis.

2.1 Wave theory

Waves come in many shapes and sizes and there are many ways to categorize the different wave types. This study will mainly focus on wind waves caused by wind blowing over the ocean surface. This subsection will discuss how wind waves are formed, how to calculate the length of the wave, how a wave spectrum is used, and how wave probability is estimated.

2.1.1 Wave forming

Folley (2017) explains that wind waves are formed when the energy in the wind is transmitted to the ocean surface. This causes small ripples that gradually grow larger until they become fully developed. Even if the wind stops blowing the waves will continue to move since the energy in the waves is conserved. Due to the low loss of energy, waves can travel far distances.

Janson (2015) states that the wave period, T, and wave height, H, are dependent on the wind speed, wind duration as well as the distance the wind can act on the waves, also known as the fetch.

Both Folley (2017) and Janson (2015) discuss how wave pressure and energy are transmitted vertically beneath the surface. The dynamic pressure and energy are highest at the surface and then decrease exponentially. This is due to that the motion amplitude of the fluid particle within the waves decreases with depth.

When analyzing waves, three parameters are used frequently, these are wave celerity, C, the wavenumber, k, and wave frequency, ω. The wavenumber is calculated using Equation 2.1 and is dependent on the wavelength, L. Wave frequency is calculated from the wave period as shown in Equation 2.2. The wave celerity is the velocity the wave is moving with and it is calculated using both the wavelength and the wave period according to Equation 2.3.

$$k = \frac{2\pi}{L} \tag{2.1}$$

$$\omega = \frac{2\pi}{T} \tag{2.2}$$

$$C = \frac{L}{T} \tag{2.3}$$

2.1.2 Wavelength

As explained in Section 1.1.1, the wave period and wave height are dependent on the wind speed, duration, and fetch. However, the wavelength is never mentioned. The wavelength is dependent on the water depth and many models have been developed to calculate the wavelength.

One common method comes from linear wave theory, also known as Airy wave theory. Airy (1845) developed a model that calculates the wavelength for infinitely deep water based on the wave period and gravitational acceleration. Equation 2.4 presents the relation between the wavelength, wave period, and gravitational acceleration. In Folley (2017) and Janson (2015) the water depth, d, is considered deep when it exceeds half of the wavelength, L, i.e., $d > L/2$.

$$L = \frac{gT^2}{2\pi} \tag{2.4}$$

From linear wave theory, there are many different modifications to calculate the wavelength at a finite depth. Faltinsen (1990) developed a model for intermediate water depth which was defined as a water depth between $L/20$ and $L/2$. His model is presented in Equation 2.5 and since the wavelength is found at both sides of the equal sign the solution needs to be solved iteratively.

$$L = \frac{gT^2}{2\pi}\tanh\left(\frac{2\pi d}{L}\right) \tag{2.5}$$

For shallow water, where the water depth is less than $L/20$ Le Roux (2007) developed a model to calculate the wavelength. The model is presented in Equation 2.6 and is dependent on the wave period, T, the gravitational acceleration, g, and the water depth, d.

$$L = \sqrt{\left(\frac{gT^3}{3\pi}\right)\sqrt{g\left(\frac{gT^2}{96\pi} + d\right)}} \tag{2.6}$$

In Janson (2015), another model is also presented for shallow water that is derived from linear wave theory. The model is presented in Equation 2.7 and is dependent on the same variables as the model from Le Roux, but it is not as complex.

$$L = T\sqrt{gd} \tag{2.7}$$

Kamphuis (2000) presents a model developed by Hunt (1979) for shallow water waves according to Equation 2.8. In Hunt's equation, C is the wave celerity which is calculated from Equation 2.9, where the non-dimensional coefficient, y_0, is obtained using Equation 2.10.

$$L = TC \tag{2.8}$$

$$\frac{C^2}{gd} = y_o + \frac{1}{1 + 0.6522y_0 + 0.4622y_0^2 + 0.0864y_0^3 + 0.0675y_0^4} \tag{2.9}$$

$$y_0 = \frac{2\pi d}{L} \tag{2.10}$$

2.1.3 Wave spectrum

When analyzing wave measurements, it is common to convert the measured time series of data into the frequency domain. This can be done using Fourier transforms, creating a variance spectrum, also known as a wave-energy spectrum. The spectrum can then be smoothened and transformed into a continuous density spectrum to make comparisons with other spectrums easier. (Janson 2015)

Janson (2015) mentions that the characteristics of the waves can be estimated using spectral moments. Equation 2.11 presents the equation of spectral moments where $S(\omega)$ is the spectral variance density and ω is the wave frequency which can be obtained using Equation 2.2.

$$m_n = \int_0^\infty S(\omega)\omega^n \, d\omega \tag{2.11}$$

The wave climate at a specific location can be estimated using different theoretical spectrums. Janson (2015) mentions four different spectrums, The Pierson-Moscowitz spectrum, the ITTC spectrum, the Bretschneider spectrum, and the JONSWAP spectrum. All spectrums require different inputs and vary in complexity and accuracy.

Sadeghi (2008) disuses the generation of waves and presents Equation 2.12 and 2.13 for deep water waves and non-deep water waves. The equations are called the Sverdrup-Munk-Bretschneider equations and are the result of the modifications made to the Sverdrup-Munk equation by Bretschneider in 1958.

Equation 2.12 is derived for deep water conditions and gives the significant wave height based on the gravitational acceleration, g, the wind speed, U, and the fetch length, F. For non-deep water, Equation 2.13 is applied which depends on the same variables as Equation 2.12 as well as the water depth, d.

$$\frac{gH_s}{U^2} = 0.283 \tanh\left(0.0125\left(\frac{gF}{U^2}\right)^{0.42}\right) \tag{2.12}$$

$$\frac{gH_s}{U^2} = 0.283 \tanh\left(0.530\left(\frac{gd}{U^2}\right)^{0.75}\right)\tanh\left(\frac{0.0125\left(\frac{gF}{U^2}\right)^{0.42}}{tanh\left(0.530\left(\frac{gd}{U^2}\right)^{0.75}\right)}\right) \quad (2.13)$$

In 1976 Hasselmann developed a parametric model by simplifying the JONSWAP equation. The parametric model is presented by the Coastal Engineering Research Center (1984) as Equation 2.14. Equation 2.14 is dependent on the gravitational acceleration, g, the wind speed, U, and the fetch length, F.

$$\frac{gH}{U^2} = 0.0016\left(\frac{gF}{U^2}\right)^{0.5} \quad (2.14)$$

2.1.4 Wave probability

Another parameter used when analyzing wave climates is wave probability. Wave probability is used to evaluate the likelihood of different wave climates to find the most common wave characteristics at a specific location. Using the specific wave heights from measurements at a specific location it is possible to find the maximum theoretical significant wave height. Janson (2015) states that the probability distribution can be estimated using a Weibull distribution according to Equation 2.15.

$$P(H_s > x) = e^{-\left(\frac{x}{H_c}\right)^{\gamma}} \quad (2.15)$$

The Weibull distribution is modified by changing the values of γ and H_c until it fits well with the measured distribution. Janson (2015) presents a method that finds the values of γ and H_c so that the Weibull distribution fits well with the statistical distribution. To obtain the values of γ and H_c Equation 2.16 and 2.17 need to be solved where n_j, represents the cumulated sum of occurrences, and N_{tot}, is the total amount of readings.

$$P(H_s > i\Delta H_s) = 1 - P_i \quad (2.16)$$

$$P_i = P(H_s < i\Delta H_s) = \frac{\sum_{j=1}^{i} n_j}{N_{tot} + 1} \quad (2.17)$$

Once Equation 2.16 and 2.17 are solved the value of $\ln(-ln(1 - P_i))$ needs to be plotted against $\ln(H_s)$. Linear regression is then used to fit a straight line to the graph where the slope of this straight line is equal to γ and the position where the graph intersects with the x-axis is the natural logarithm of H_c.

Once the values of γ and H_c are found, Equation 2.18 can be used to find the maximum significant wave height during a specific time frame. N_o represents the number of observations and it is this parameter that determines the time frame. Equation 2.19 is used to calculate the number of observations and it is dependent on the variable T_{years} which defines the number of years of interest and T_{sample} which is the time between each sample in hours for the measurement.

$$H_{s,max} = H_c \sqrt[\gamma]{\ln(N_o)} \tag{2.18}$$

$$N_0 = 8766 \cdot T_{years} \cdot T_{sample} \tag{2.19}$$

Using the theoretical maximum significant wave height, Janson (2015), presents a simple formula to evaluate the theoretical maximum wave height. Equation 2.20 presents this formula where H_s is the maximum significant wave height obtained from Equation 2.18 and N is the number of waves in the sample.

$$H_{max} = H_s \sqrt{\frac{1}{2}\ln(N)} \tag{2.20}$$

2.2 Wave transmission

The transmission coefficient is the most common method to evaluate the performance of floating breakwaters. Many different theoretical models have been developed to predict the wave transmission of different breakwaters. Since the different types of breakwaters behave differently, they require different models. This study is focusing on the SFBW1000(3.0) breakwater from SF-marina which is a Π-type pontoon breakwater.

This study will not only look at theoretical models developed for the Π-type breakwater. The wings that extend down from the breakwater can be seen as a vertical rigid barrier if the waves are small and hence some models developed for that breakwater type will be used. Since the rough shape of the breakwater is a floating box, theoretical models developed for box-shaped floating breakwaters will also be analyzed.

2.2.1 Vertical rigid barrier

The vertical rigid barrier is a breakwater type that has a thin plate that extends down from some distance above the water surface to a distance below the surface. Wiegel (1960) developed a theoretical model based on a model from Ursell (1947). In this model Wiegel (1960) assumed that the power transmitted through the breakwater is the power that can pass through between the sea bottom and the breakwater.

In Wiegel (1992), the equation from Wiegel (1960) is presented as Equation 2.21, which is dependent on the water depth, d, the draft of the breakwater, D, and the wavelength, L.

$$c_{t,W} = \sqrt{\frac{\left(\frac{\frac{4\pi(d-D)}{L}}{\sinh\left(\frac{4\pi d}{L}\right)} + \frac{\sinh\left(\frac{4\pi(d-D)}{L}\right)}{\sinh\left(\frac{4\pi d}{L}\right)}\right)}{1 + \frac{\frac{4\pi d}{L}}{\sinh\left(\frac{4\pi d}{L}\right)}}} \tag{2.21}$$

Kriebel and Bollmann (1996) further researched the model from Wiegel (1960) by also considering the wave reflection. They assumed that the pressure beneath the breakwater is the sum of the incoming wave pressure and the reflected wave pressure. Using this assumption, they presented a correction to Wiegel (1960). The correction is presented in Equation 2.22.

$$c_{t,WR} = \frac{\left(2c_{t,W}^2\right)}{\left(1 + c_{t,W}^2\right)} \tag{2.22}$$

From an internal document at SF-Marina another correction equation is presented. This correction takes into account that the breakwater from SF-Marina is not as thin as the vertical rigid barrier. This model is based on some work from Cox in 1987 but no source has been found to support this. The correction is presented in Equation 2.23 where the effective breadth, B_e, can be calculated using Equation 2.24. The effective breadth is dependent on the breadth of the breakwater, B, and the angle, α, between the wave and breakwater.

$$c_{t,WB} = c_{t,W} \cdot \left(\frac{\left(2\sqrt{\left(1 + \left(\frac{(2\pi B_e)}{L}\right)^2\right)}\right)}{\left(2 + \left(\frac{(2\pi B_e)}{L}\right)^2\right)}\right) \tag{2.23}$$

$$B_e = \frac{B}{\cos(\alpha)} \tag{2.24}$$

The internal documentation from SF-Marina also presents a model that is based on the work from Kriebel (2000). The study from Kriebel (2000) evaluates the performance of vertical rigid barriers in random waves. Kriebel (2000) predicts the performance using a modified eigenfunction expansion theory that takes into account the frictional losses. The predicted performance is then compared to measured data from laboratory experiments and the results are presented in a graph.

The graph presents the transmission coefficient at different relative wave barrier drafts, D/L, where D is the draft of the wave barrier and L is the wavelength. The internal documentation from SF-Marina presents Equation 2.25 which, when plotted, matches the graph from Kriebel (2000).

$$c_{t,K} = \mathrm{e}^{-15\left(\frac{D}{L}\right)^{1.4}} \tag{2.25}$$

Within the internal documentation, Equation 2.25 is corrected for both reflection and breadth using Equation 2.22 from Kriebel and Bollmann (1996), and Equation 2.23 from the internal documentation. The corrected value is obtained using Equation 2.26.

$$c_{t,KRB} = \frac{2c_{t,K}^2}{1 + c_{t,K}^2} \cdot \left(\frac{\left(2\sqrt{\left(1 + \left(\frac{(2\pi B_e)}{L} \right)^2 \right)} \right)}{\left(2 + \left(\frac{(2\pi B_e)}{L} \right)^2 \right)} \right) \tag{2.26}$$

2.2.2 Box-shaped floating breakwater

The box-shaped floating breakwater is a rectangular box that floats on the surface and is held in place using an anchoring system. These breakwaters do not include the downward-facing wings as the Π-type breakwaters and thus roll motions are not dampened as much. Carr (1951) described the motion of the box-shaped breakwater with elastic anchoring lines using the equation of dynamics. Tsinker (1995) stated that the model from Carr (1951) was suitable for shallow water wave conditions where the relative wave height, H/L, is not exceeding 0.04. Equation 2.27 presents Carr's equation as it is presented in Tsinker (1995).

$$c_{t,C} = \frac{1}{\sqrt{1 + \left[\left(\frac{\pi B}{L} \right) \cdot \left(1 + \frac{D}{d - D} \right) \right]^2}} \tag{2.27}$$

Two years after Carr presented his model, Macagno (1953), presented an analytical formula for box-shaped breakwaters that are rigidly moored. Dai et al. (2018) stated that the model from Macagno (1953) is based on linear wave theory, assuming that the breakwater is stationary in the water. It also assumed constant water depth and that there is no green water on top of the breakwater.

Ruol et al. (2013) also discussed the model from Macagno (1953). They state that the model is derived for an infinitely long breakwater that is subjected to regular waves and does not take into account any reflected waves. In Tsinker (1995), the formula from Macagno was presented as Equation 2.28 where, k, is the wavenumber of the incoming wave, B, is the breadth of the breakwater, d, is the water depth, and D, is the breakwater draft.

$$c_{t,M} = \frac{1}{\sqrt{1 + \left[\frac{k\,B\sinh(k_i d)}{2\cosh(k\,d - k\,D)}\right]^2}} \tag{2.28}$$

2.2.3 Floating Π-type breakwater

The Π-type breakwater has two downward-facing wings at the sides of the breakwaters to increase the efficiency of the breakwater. Ruol et al. (2013) developed a correction of the model from Macagno (1953) to better fit the Π-type breakwater. They introduced a dimensionless correction equation $\beta(\chi)$ which can be seen in Equation 2.29, where the dimensionless equation $\beta(\chi)$ is calculated using Equation 2.30.

$$c_{t,R} = \beta(\chi) \cdot c_{t,m} \tag{2.29}$$

$$\beta(\chi) = \frac{1}{1 + \left(\frac{\chi - \chi_0}{\sigma}\right) e^{-\left(\frac{\chi-\chi_0}{\sigma}\right)^2}} \tag{2.30}$$

The correction equation $\beta(\chi)$ depends on the constants χ_0 and σ as well as the variable χ which is a scaling parameter that is obtained using Equation 2.31.

$$\chi = \frac{T_p}{2\pi}\sqrt{\frac{g}{D + 0.35B}} \tag{2.31}$$

The correction equation is developed by comparing the transmission coefficient calculated with the formula from Macagno with measured data. The results are presented in a graph where the transmission coefficient is given for different values of the scaling parameter. Using the graph from Ruol et al. (2013) the values of the constants in Equation 2.30 are derived as:

$$\chi_0 = 0.7919$$

$$\sigma = 0.1922$$

Günaydin and Kebdaşli (2007) investigated the performance of solid and perforated, Π-type floating breakwaters. They carried out experiments with models of different sizes and developed a model for predicting the transmission coefficient using the Buckingham PI theorem. Equation 2.32 presents the model, which is dependent on the coefficients M_{GK}, N_{GK}, Par_1 as well as the wavelength, L, the water depth, d, and the draft, D.

$$c_{t,GK} = \left(M_{GK}(Par_1)^{N_{GK}} \frac{L}{d-D}\right)^2 \tag{2.32}$$

The coefficients m and n are obtained from experimental testing and the coefficient Par_1 is obtained using Equation 2.33. Par_1 is dependent on the wave height of the incoming waves, H_i, as well as the wavelength, L, the water depth, d, and the draft, D.

$$M_{GK} = 0.6685$$

$$N_{GK} = 0.2067$$

$$Par_1 = \frac{H_i^2(d-D)}{L^3} \tag{2.33}$$

The Buckingham Pi theorem was also used by Moghim and Botshekan (2017) to develop a theoretical model for predicting the performance of a Π-type floating breakwater for a 2D wave. The non-dimensional variables are derived differently when compared to the model from Günaydin and Kebdaşli (2007) and the values of the coefficients are obtained using many different experimental studies. Equation 2.34 presents the model from Moghim and Botshekan (2017) which is dependent on the draft, D, the incoming wave height, H_i, the breadth, B, the gravitational acceleration, g, and the wave period, T.

$$c_{t,MB} = 0.05\left(\frac{DH_i}{B^2}\right)^{-0.2}\left(\frac{gT^2}{B}\right)^{0.6} \tag{2.34}$$

2.2.4 Summary of transmission models

In total, 11 different theoretical models for predicting the wave transmission coefficient are found. All are derived differently and include different assumptions and variables. A summary of all models is presented in Table 2.1 where the name, notation, dependent variables, equation number, and the source is presented for each model.

Table 2.1 Summary of transmission models

Name	c_t	Dependent variables	Equation number	Source
Wiegel 1960	$c_{t,W}$	d, D, L	2.21	Wiegel (1992)
Wiegel 1960 with reflection correction	$c_{t,WR}$	$c_{t,W}$	2.22	Kriebel and Bollmann (1996)
Wiegel 1960 with breadth correction	$c_{t,WB}$	$c_{t,W}, L, B, \alpha$	2.23	Internal documentation at SF-Marina
Wiegel 1960 with reflection and breadth correction	$c_{t,WRB}$	$c_{t,W}, L, B, \alpha$		Internal documentation at SF-Marina
Kriebel 2000	$c_{t,K}$	D, L	2.25	Kriebel (2000)
Kriebel 2000 with reflection and breadth correction	$c_{t,KRB}$	$c_{t,K}, L, B, \alpha$	2.26	Internal documentation at SF-Marina
Carr 1951	$c_{t,C}$	d, D, L, B	2.27	Tsinker (1995)
Macagno 1953	$c_{t,M}$	k, d, D, B	2.28	Tsinker (1995)
Ruol et al. 2013	$c_{t,R}$	$c_{t,M}, T, g, B, \chi_0, \sigma$	2.29	Ruol et al. (2013)
Günaydin and Kebdaşli 2007	$c_{t,GK}$	d, D, L, H_i, M, N	2.32	Günaydin and Kebdaşli (2007)
Moghim and Botshekan 2017	$c_{t,MB}$	D, H_i, B, g, T	2.34	Moghim and Botshekan (2017)

2.3 Breakwater movement

Since the breakwater is moored with chains and anchors it can translate in the three principal directions and rotate around the three principal directions as well. This results in 6 degrees of freedom, heave, sway, surge, roll, pitch and yaw. In Figure 2.1 a simplified breakwater is shown with the principal axes and the heave, sway and surge direction. Roll is defined as the rotation around the x-axis and is denoted with ϕ, the pitch is the rotation around the y-axis and is denoted as θ, and the yaw is the rotation around the z-axis, denoted as ψ.

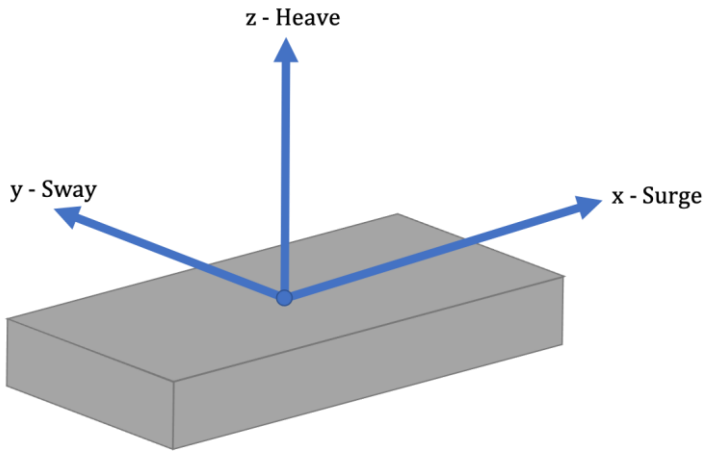

Figure 2.1 Degrees of freedom of breakwater.

2.3.1 Strip theory

One hypothesis is that strip theory might be possible to use to determine the performance of a floating breakwater. According to Janson (2015), the strip theory is primarily used for the motion analysis of ship hulls. The theory is based on that the hull is divided into a finite number of two-dimensional strips and then the coefficients for added mass, dampening, and restoring forces are solved for each strip. The coefficients are then summated over all the strips to get the coefficients of the complete hull.

One way of obtaining the added mass and damping coefficients for roll and sway is using Lewis forms. Lewis forms are based on analytical solutions and determine the coefficients using two parameters, the beam to draft ratio and the sectional area coefficient.

Strip theory is based on several assumptions but according to Janson (2015), the theory might still be valid even if some of the assumptions are not fulfilled. The first assumptions are that the hull is rigid and that it is considered slender. Moderate speed and small motions are also assumed for the hull as well as wall-sided hull sections and deep water.

2.3.2 Natural roll frequency

The breakwater structure has a natural roll frequency that will affect the movement of the breakwater. Cederwall and Larsen (1979) present Equation 2.35 as a method of determining the natural period, T_n, of a floating structure. In Equation 2.35, I_m, is the moment of inertia around an axis of the floating breakwater, P, is the mass of the structure in newton, and H_m, is the metacentric height in meters of the floating breakwater.

$$T_n = 2\pi \sqrt{\frac{I_m}{PH_m}} \tag{2.35}$$

3 Method

This study is using a wave recorder and an Arduino IMU motion sensor to gather data about the performance of the floating breakwater. The limitations and details of the instruments are presented here together with information about the deployment of the instruments. The expected output variables of the instruments are explained together with how to filter the obtained data to get more accurate results in the analysis.

To get a good understanding of the wave climate this section explains how wind data is obtained. The wind data is compared with the wave data from the wave recorders. This section also explains the commercial software, Ansys AQWA, that is compared with the data from the wave recorders.

3.1 Wave climate

The transmission coefficient depends on the incoming wave height and the transmitted wave height as shown in Equation 1.1. Using two wave recorders, the wave height on both sides of the breakwater can be measured. By analyzing this data and comparing it to the theoretical data, the most suitable theoretical model can be determined.

3.1.1 Wave recorder

The wave recorders used for this study are of the model MIDAS DWR from Valeport limited. DWR stands for directional wave recorder and implies that the recorder can sense the direction of the waves as well as the magnitude. The wave recorder uses linear wave theory and measures pressure variations caused by the waves as well as current oscillations caused by the movement of the waves. (Valeport Limited 2008)

Pressure is measured using a piezoresistive transducer with a 100 dBar range and an accuracy of 0.01% (Valeport Limited 2008). Folley (2017) as well as Valeport Limited (2008) states that this type of wave recorder is suitable for water depths less than 20m.

The wave direction is measured using the Valeport 11cm discus electromagnetic sensor. It measures the wave direction by analyzing the current oscillation caused by the motion of the waves and it is capable of measuring currents up to 5m/s in either direction. The accuracy of the sensor is +/- $1\% + 5mm/s$ and the readings from the sensor have a resolution of 0.001m/s. (Valeport Limited 2008)

The direction of the wave recorder is defined using an inbuilt fluxgate compass. By using this compass, the orientation of the wave recorder can be determined with a resolution of 0.1° and an accuracy of +/- 1%. (Valeport Limited 2008)

The instrument uses a wave burst measurement system meaning that it will measure the pressure for a predefined time and then wait some time before the next wave burst. Using this method ensures that the inbuilt memory and batteries last longer. When setting up the sample time, and waiting time, it is important to remember that more samples in the burst will give a more accurate measurement, but the instrument will not be able to run for as long. On the other hand, fewer samples will make the batteries and memory last longer with a less accurate result. (Valeport Limited 2008)

For long-time deployment when analyzing the wave climate Valeport Limited (2008) recommends having a sample time of 1024 seconds (~17 minutes) with a measurement frequency of 1 Hz and measuring every second hour. For the first deployments of the wave recorders, these recommendations had not been found and the instrument was set up according to Table 3.1.

Table 3.1 Setup of wave recorders for wave climate measurements.

Deployment date	Days deployed	Sample time [sec]	Sample frequency [Hz]	Waiting time between samples [min]
2020-11-20	47	64	8	22
2021-01-29	47	64	8	22
2021-03-18	49	1024	2	88

3.1.2 Deployment site

Since the instrument measures the pressure at the bottom, the accuracy of the measurements will be dependent on the water depth. At Skärhamn the water depth is approximately 10m and according to the operating manual from Valeport Limited (2008), the shortest wave period the instrument will be able to detect is around 3.7s.

When choosing the deployment site, Valeport Limited (2008) states that it is important to avoid placing the recorder in areas where waves are reflected. This causes faulty measurements as the reflected waves distort the incoming waves. The wave recorders are positioned according to Figure 3.1 where A is positioned around 40-50 meters outside of the breakwater and B is positioned 10-20 meters inside of the breakwater.

When measuring the pressure at the bottom, high-frequency distortions might be picked up by the sensor. To get rid of these distortions a filter is used. However, using this filter means that high-frequency waves that are picked up by the sensor also are removed. (Valeport Limited 2008)

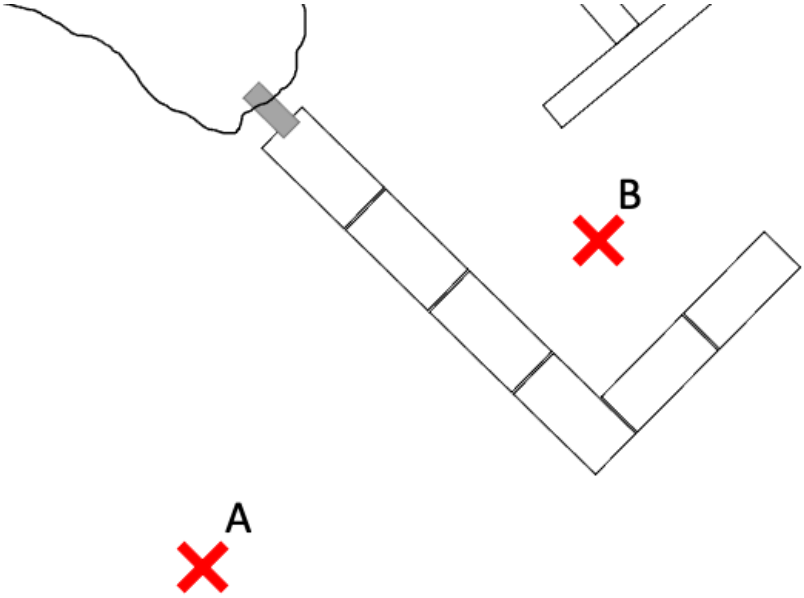

Figure 3.1 Positions of wave recorders.

The maximum and minimum wave frequency that can be picked up can be calculated using Equations 3.1 and 3.2. $N_{spectral}$ is the number of spectral points which is calculated using Equation 3.3, f_{res}, is the frequency resolution calculated using Equation 3.4, T_{sample}, is the sample time, and N_{sample}, is the number of samples in one wave burst. (Valeport Limited 2008)

$$f_{max} = f_{res}\left(N_{spectral} - 1\right) + f_{min} \tag{3.1}$$

$$f_{min} = 0.5 \cdot f_{res} \tag{3.2}$$

$$N_{spectral} = \frac{5N_{samples}}{128} - 1 \tag{3.3}$$

$$f_{res} = \frac{8}{T_{sample}} \tag{3.4}$$

Applying these equations to the setups presented in Table 3.1 the frequency resolutions in Table 3.2 are obtained. However, the water depth of the deployment site will affect the lowest measurable wave period.

Table 3.2 Frequency resolution of wave climate measurements

Deployment date	$N_{samples}$	T_{sample} [sec]	f_{res} [Hz]	f_{min} / T_{max} [Hz] / [sec]	f_{max} / T_{min} [Hz] / [sec]
2020-10-20	512	64	0.125	0.0625 / 16	2.3125 / 0.43
2021-01-29	512	64	0.125	0.0625 / 16	2.3125 / 0.43
2021-03-18	2048	1024	0.0078	0.0039 / 256	0.61 / 1.63

3.1.3 Data processing

When processing the pressure data from the wave recorders, many different parameters are obtained. Since the tide at Skärhamn is negligible it is only the parameters related to waves that will be used. These are:

- Mean water height, $\bar{d}$
  The mean water height is obtained by measuring the absolute pressure at the wave recorder. This includes both the air pressure at the deployment site as well as the static water pressure.

- Significant wave height, H_s
  The significant wave height is obtained from the spectral moments of the wave samples. It is calculated using Equation 3.5 where, $m_0^{1/2}$, is the standard deviation of the surface elevation.

$$H_s = 4 \cdot m_0^{1/2} \tag{3.5}$$

- Maximum wave height, H_{max}
  The maximum wave height is based on the significant wave height. In the operating manual from Valeport Limited (2008), it is stated that the equation used comes from Goodknight and Russel (1963) and that there also exist other equations that can be used. The equation used is presented in Equation 3.6.

$$H_{max} = 1.57 \cdot H_s \tag{3.6}$$

- Mean wave period, T_1
  The mean wave period is the mean of all wave periods and it is calculated using the spectral moments of the surface elevation according to Equation 3.7.

$$T_1 = \frac{m_0}{m_1} \tag{3.7}$$

- Mean zero up-crossing period, T_z
  The mean zero up-crossing period is the mean time between each passing of the ocean level through the mean water level. It is evaluated from spectral moments of the time series of surface elevation using Equation 3.8.

$$T_Z = \left(\frac{m_0}{m_2}\right)^{\frac{1}{2}} \tag{3.8}$$

- Peak period, T_p
  The peak period is obtained from the wave spectrum and it relates to the period where the peak energy is located.

- Significant period, $T_{1/3}$
  The significant period is calculated using Equation 3.9 from Valeport Limited (2008) which uses the peak period, T_p.

$$T_{1/3} = 1.02 \cdot T_p \tag{3.9}$$

- Total energy, E
  The total energy is calculated using Equation 3.10 which depends on the significant wave height, the density of the water, and the gravitational acceleration. The unit of the total energy is thus N/m or J/m^2 which is not the common unit of energy (J). Thus, the equation rather gives the energy density in the wave.

$$E = \frac{\rho g H_s^2}{16} \tag{3.10}$$

- Mean wave direction
  The mean direction of the waves is based on the energy distribution and gives the direction of the waves, weighted by the energy within the wave.

The wave climate is measured both on the inside and outside of the breakwater, making it possible to analyze how the breakwater affects the wave climate and how the breakwater performs in different conditions.

3.2 Wind data

To evaluate how the wind and waves correlate in Skärhamn, it is necessary to obtain wind data close to the breakwater location. Wind data from that region can be obtained from either the Swedish Meteorological and Hydrological Institute (SMHI) or ELJI electronics which is a Swedish distributor of weather stations from Davis Instruments.

SMHI (n.d.) has a weather station at Måseskär which is located about 17km northwest of Skärhamn. From SMHI (n.d.) it is possible to obtain the mean wind speed and direction for every hour.

ELJI electronics (n.d.) has a weather station in Säby which is located about 4.5km northeast of Skärhamn. From that weather station, it is possible to get the same data as from SMHI (n.d.), i.e., the mean wind speed as well as the dominant direction of the wind. However, ELJI electronics (n.d.) only has a daily average of the wind data and not an hourly average as SMHI (n.d.) has.

3.3 Breakwater movement

To analyze the movement of the breakwater and how the movement affects the performance of the breakwater, an Inertial Measurement Unit (IMU) is used. The IMU is connected to an Arduino where the data from the IMU is logged onto an SD card. The data can then be filtered to obtain the motions of the breakwater.

3.3.1 Arduino IMU sensor

The sensor consists of an Arduino Uno Rev 3 SMD with an ATmega328 microcontroller (Arduino, n.d.). The objective of the microcontroller is to obtain the values from the IMU and saving them onto an SD card together with a time stamp. Connected to the Arduino Uno is a data logger shield from Adafruit. This shield contains an RTC (Real Time Clock) and an SD card reader/writer that enables the microcontroller to store data onto a regular SD card. (Adafruit, 2021)

An IMU measures motions using a magnetometer, a gyroscope, and an accelerometer. For this study, the LSM9DS1 IMU from STMicroelectronics is used, mounted on a breakout board from Sparkfun to simplify connections. (Sparkfun, 2015)

A magnetometer measures the magnetic field and can give the relation of the sensors to the magnetic north. This sensor is thus able to sense the yaw motion of the breakwater. It measures the angle in Gauss (Gs) and when setting up the instrument it is possible to set the scale to either 4, 8, 12, or 16 Gs. (Sparkfun, 2015) The scale affects the resolution of the readings. For this application, the standard scale of 12 Gs is used.

An accelerometer measures the linear acceleration in the unit of gravitational acceleration (g). When stationary it will sense the direction of gravity and can thus be used both to sense angular changes and translations. It is suitable for measuring slow movements and bad at detecting rapid changes. The measurement scale can be set to 2, 4, 8, or 16g and for this application, a scale of 8g is used.

Accelerometers are suitable to use to find the roll and pitch angles, but it is not possible to obtain yaw angles. To find the angles of the roll and pitch, Equations 3.11 and 3.12 are used where the accelerometer output (a_x, a_y and a_z) is combined to get the unknown angles. (MATLAB, 2018)

$$\phi_{acc} = \operatorname{atan}\left(\frac{a_y}{\sqrt{a_x^2 + a_z^2}}\right) \tag{3.11}$$

$$\theta_{acc} = \operatorname{atan}\left(\frac{a_x}{\sqrt{a_y^2 + a_z^2}}\right) \tag{3.12}$$

A gyroscope measures the rotational acceleration in degrees per second (DPS). It is suitable for sensing the rotations of the breakwater and it is good at detecting rapid movements. When interpolating the output from the gyroscope from degrees per second to degrees the angle tends to drift. When setting up the instrument it is possible to use a scale of 245, 500, or 2000 DPS and for this application, a scale of 245 DPS is used.

3.3.2 Data filtering

The different sensors within the IMU have different advantages and disadvantages. By combining the readings from the different sensors, a more accurate result is obtained than what each sensor would produce. Many different filters can be used to accomplish this, and the different filters have varying accuracy and complexity.

A complementary filter is commonly used to combine accelerometer, magnetometer, and gyroscope data. In a complementary filter, the accelerometer and magnetometer data are passed through a low pass filter and the gyroscope data is passed through a high pass filter. The filtered data from the different sensors are then added together to get the roll, pitch, and yaw angles. (MATLAB, 2018)

According to Thomson and Emery (2014), the running mean filter is commonly used as a low pass filter for oceanography, and it is simple to implement. The filter is suitable for situations where we have already measured data since it calculates a mean value based on data points both before and after. Equation 3.13 presents the general equation for the running mean filter where M is the number of data points ahead, and behind, the data point to be filtered. A higher value of M filters the data more and a smaller value of M filters the data less.

$$\bar{\phi}_{low} = \frac{1}{2M+1} \cdot \sum_{k=-M}^{M} \phi_k \tag{3.13}$$

The running mean filter is a low-pass filter but according to Thomson and Emery (2014) all low-pass filters can be converted into high pass filters by removing the filtered value from the original value, this is done in Equation 3.14.

$$\bar{\phi}_{high} = \phi - \bar{\phi}_{low} \tag{3.14}$$

Accelerometers and magnetometers produce noise when active but are at the same time very accurate in the long term. I.e., the low frequencies are accurate from the accelerometer and magnetometer but the high frequencies might contain errors. By using a running mean filter over the data from the accelerometers and magnetometers the high frequencies will be attenuated and only the low frequencies will be left.

The gyroscope is more accurate for the high frequencies but is prone to drift and thereby not accurate for the lower frequencies. Thus, a high pass filter is suitable to reduce the low frequencies and keep the high frequencies. Using Equation 3.14 will accomplish this and to get the final angles of the breakwater the filtered values from the accelerometer, magnetometer and gyroscope can then be added together according to Equations 3.15, 3.16, and 3.17.

$$\phi = \bar{\phi}_{accelerometer} + \bar{\phi}_{gyroscope} \tag{3.15}$$

$$\theta = \bar{\theta}_{accelerometer} + \bar{\theta}_{gyroscope} \tag{3.15}$$

$$\psi = \bar{\psi}_{magnetometer} + \bar{\psi}_{gyroscope} \tag{3.17}$$

3.4 Suitable software

One objective of the study is to find suitable software that can be used to estimate the performance of a floating breakwater. Ansys AQWA is a software that is capable of investigating the effect of wind, waves, and currents on floating and fixed structures in an ocean environment. The software is divided into two packages, hydrodynamic diffraction, and hydrodynamic time response. (Ansys 2012)

Hydrodynamic diffraction is used to develop primary hydrodynamic parameters that are required to solve complex motion and response analyses. The hydrodynamic diffraction package solves three-dimensional radiation and diffraction for multiple bodies while also taking into account the interaction effect between the bodies. (Ansys 2012)

Hydrodynamic time response uses the results from the hydrodynamic diffraction to further analyze the dynamics of the structure. In the time response, it is possible to add anchoring lines and other physical connections between structures and between a structure and a fixed point in space. (Ansys 2012)

When carrying out a hydrodynamic diffraction analysis in Ansys AQWA the first step is to model the shape of the hull in Ansys 3d modeling software. The main dimensions of the model in Ansys use the values presented in Table 1.3 and the only difference between the real model and the model in Ansys is that the fins have double thickness due to mesh restrictions in the software.

Three separate structures are then connected in the same fashion as they are connected in Skärhamn and the center of gravity and moment of inertia from Table 1.3 are added to each structure. After setting up the proper analysis settings it is possible to get a surface plot showing the surface elevation.

To obtain the exact values of the surface elevation the field points approach needs to be implemented. The field points approach includes a non-physical surface in the model that is placed at the water level. The surface is made fixed in space and by analyzing the pressure at the nodes of this structure it is possible to obtain the wave amplitude at that position. (Akhemka 2020)

4 Result

This section presents the results from the wave recordings and how they are filtered for analysis. Wave probability from the recordings is presented and fitted to a theoretical probability distribution to find the theoretical maximum wave height in Skärhamn for different periods.

Wind recordings are compared with the wave recordings to find relations between the wind and incoming wave climate at the location and the wavelength is calculated using different theoretical formulas. The wave transmission is compared with different incoming wave characteristics to find what parameters the transmission is dependent on.

The results from the theoretical models presented in Section 2.2 are presented together with the result from the Ansys AQWA software which was discussed in Section 3.4. The wave data is also compared with the IMU data recorded on the breakwater to evaluate if there is any correlation between different wave parameters and breakwater movement.

4.1 Wave climate

The wave climate was measured using the wave recorders presented in Section 3.1.1, during the periods presented in Table 3.1. During the first measurement, the two wave recorders were out of sync meaning that the instruments did not measure the climate at the same time. The recorder on the inside measured the wave climate 10 minutes after the one on the outside.

During the second measurement, there were times where ice was formed on the surface which caused faulty measurements from the wave recorders as the ice dampens the incoming waves. By analyzing the ocean temperature from the oceanographic stations presented in Table 4.1 it is possible to assess the possibility of ice forming.

Table 4.1 Oceanographic stations used to evaluate ocean temperature

Station name	Distance from Skärhamn
Marstrand SJÖV	12 km south of Skärhamn
Brofjordens WR BOJ	35 km north-west of Skärhamn
Brofjordens SJÖV	40 km north of Skärhamn

Figure 4.1 presents the mean temperature for the stations mentioned in Table 4.1 and by analyzing this graph it is seen that the ocean temperature is above 0 °C after the 23rd of February. Hence after the 23rd of February, the risk of ice is smaller, and only wave data obtained after that date will be used in the analysis. Data points that were considered unphysical were also removed from the data to improve the accuracy of the result.

Figure 4.1 Mean ocean temperature during the second measurement (SMHI n.d.).

4.1.1 Wave probability

The wave probability is analyzed to find the most common wave climates in Skärhamn. For this analysis only values from the wave recorder located on the outside of the breakwater are used, instrument A in Figure 3.1. The wave direction distribution is presented in Figure 4.2 where the data is divided into 13 separate groups, 30° apart. The probability at each column thus has a resolution of ±15°. About 95.6% of the data is located between 195° and 285°.

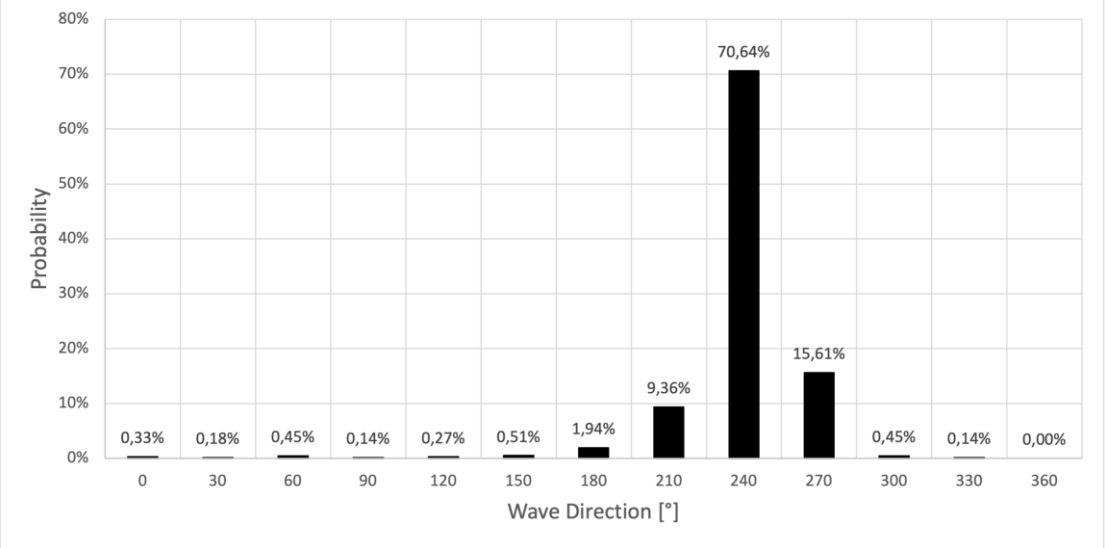

Figure 4.2 Probability of different wave directions.

In Figure 4.3 the probability distribution of the significant wave heights is presented. The significant wave heights are divided into 13 groups with a resolution of ±0.05 meters from 0.00 to 1.20 meters. 97.8% of the wave bursts had a significant wave height less than 0.45 meters with the majority between 0.00 and 0.05 meters. The mean significant wave height is 0.12 meters.

The wave period distribution is presented in Figure 4.4 and the wave period is divided into 17 groups with a resolution of ±0.25 seconds. Due to the water depth at the site, there are no waves with a period of less than 3 seconds due to the reasons explained in Section 3.1.2. Around 90.6% of the wave bursts have a mean period between 3.25 and 4.75 seconds with a majority of the wave bursts at around 3.5 seconds. The average of the mean wave periods of all wave bursts is 3.96 seconds.

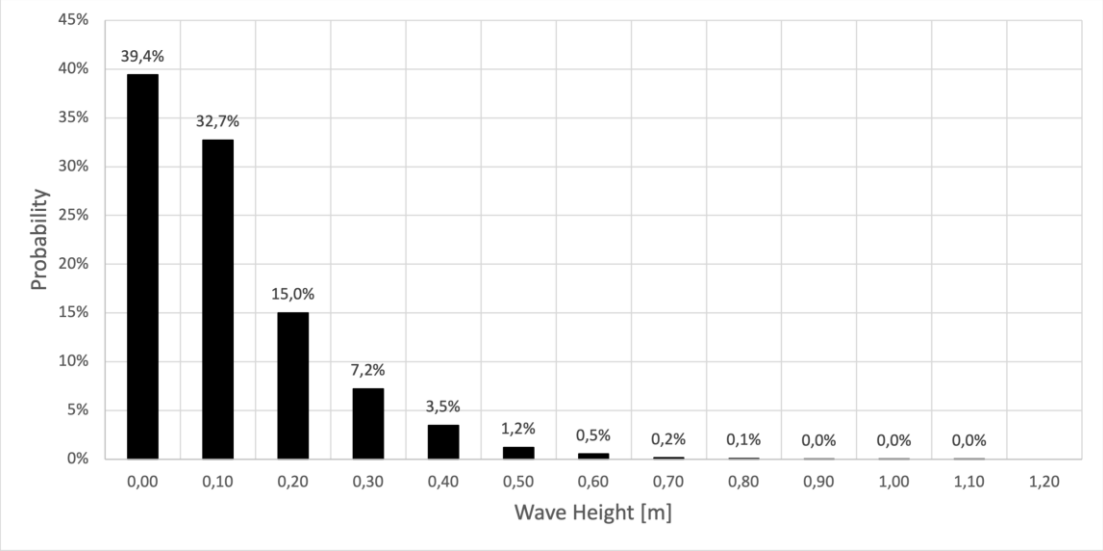

Figure 4.3 Probability of different significant wave heights.

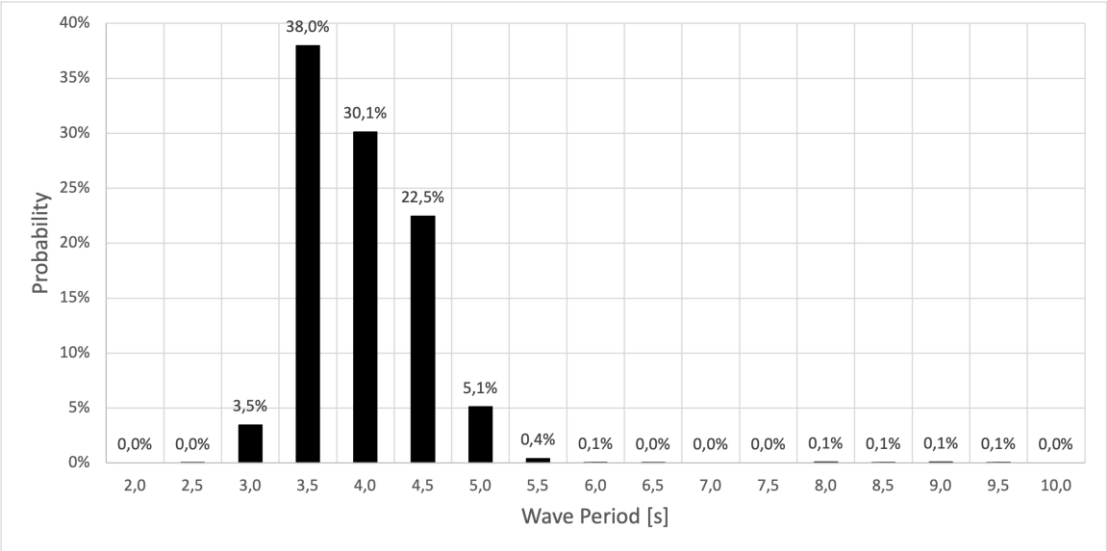

Figure 4.4 Probability of different mean wave periods.

The wave climate is a combination of the mean wave period and significant wave height. In appendix A, a table is presented which shows the probability of different combinations of mean wave period and significant wave height. This table is using the same division of the periods and heights that are used for Figure 4.3 and Figure 4.4. Table 4.2 presents the combinations that have the highest probability.

Table 4.2 Five most common wave climates from measurements

Number	Period [s]	Height [m]	Probability
1	3.5	< 0.05	16.0 %
2	3.5	0.1	13.2 %
3	4.0	< 0.05	10.8 %
4	4.0	0.1	9.7 %
5	4.5	< 0.05	7.6 %

4.1.2 Theoretical probability

The theoretical probability of wave heights is obtained using the method as explained in Section 2.1.4. The calculation of γ and H_c is presented in Appendix B and the values are found to be 0.97 and 0.11 respectively. In Figure 4.5 the statistical probability of a wave larger than a given value is compared with the theoretical probability obtained using Equation 2.15.

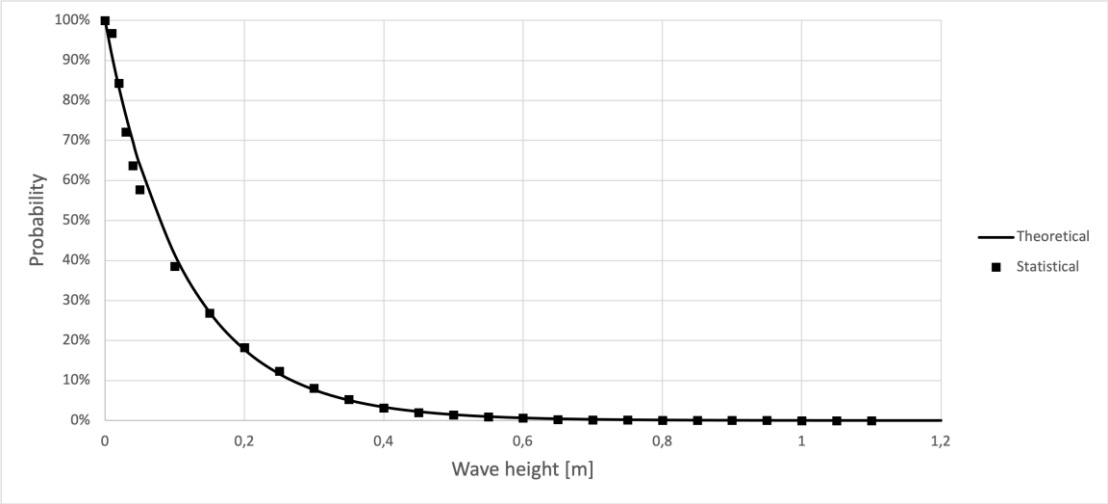

Figure 4.5 Theoretical and the statistical probability of significant wave height exceeding given height.

It is seen that the solid line, representing the theoretical probability, fits well with the squares which represent the statistical data. It is therefore assumed that this Weibull distribution can be used to evaluate the theoretical maximum wave height.

The theoretical maximum significant wave height is calculated using Equation 2.18 from Section 2.1.4 for multiple periods to obtain the dashed line in Figure 4.6. The solid line in Figure 4.6 presents the maximum theoretical wave height for the significant wave height for that period. This result is obtained using Equation 2.20. The complete calculation is presented in appendix A.

The highest obtained significant wave height during the measurements was obtained on the 22nd of February 2021 and was measured to be 1.13 meters. Comparing this with the theoretical results yields that the obtained significant wave height represents the 3.5-year wave. Meaning that a wave sequence with a significant wave height of 1.3 meters occurs once every three and a half years.

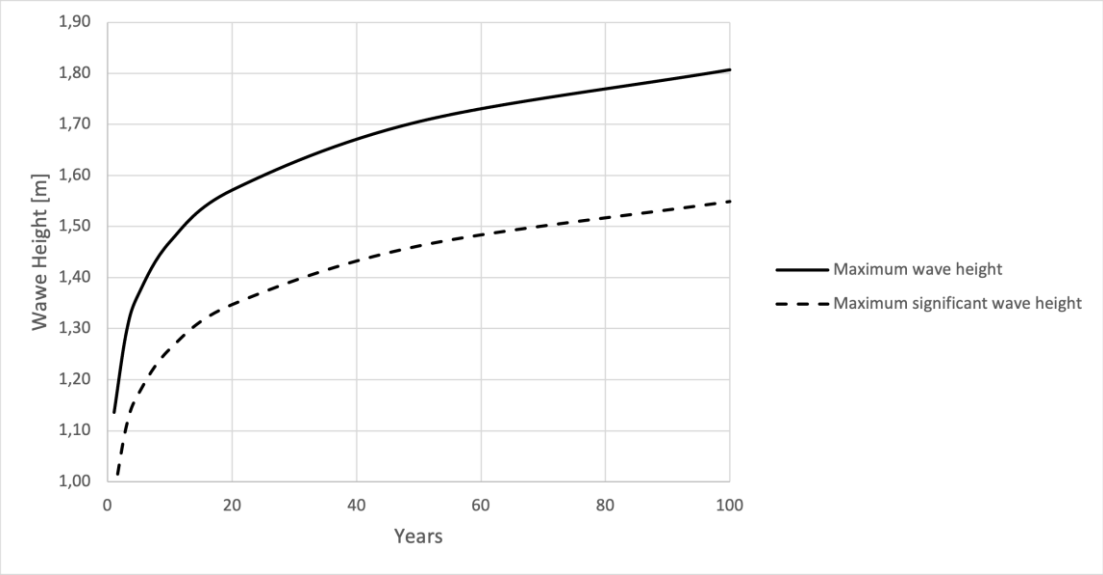

Figure 4.6 Theoretical maximum significant wave height and wave height based on Weibull distribution.

4.1.3 Wind and wave relation

As stated in Section 2.1.1 there is a relation between the wave characteristics and wind characteristics. Using the measured wave characteristics from the wave recorders and the wind data obtained from SMHI and ELJI, as explained in Section 3.2, it is possible to find correlations between the speed and direction of the wind and the height, period, and direction of the waves.

Figure 4.7 presents the relation between the significant wave height and wind speed from SMHI. From the graph, it is seen that the significant wave height increases with increased wind speed and this is also seen when comparing the significant wave height with the wind speed from ELJI in Figure 4.8. The significant wave height in the graphs is an hourly average for the SMHI wind data in Figure 4.7 and a daily average for the ELJI wind data in Figure 4.8.

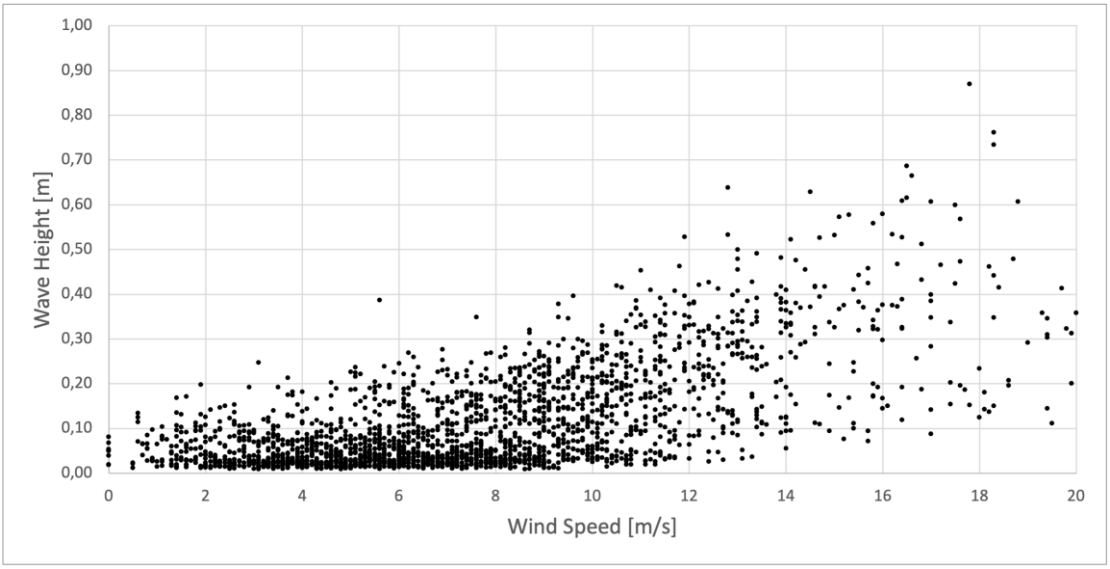

Figure 4.7 Wave height in relation to wind speed from SMHI.

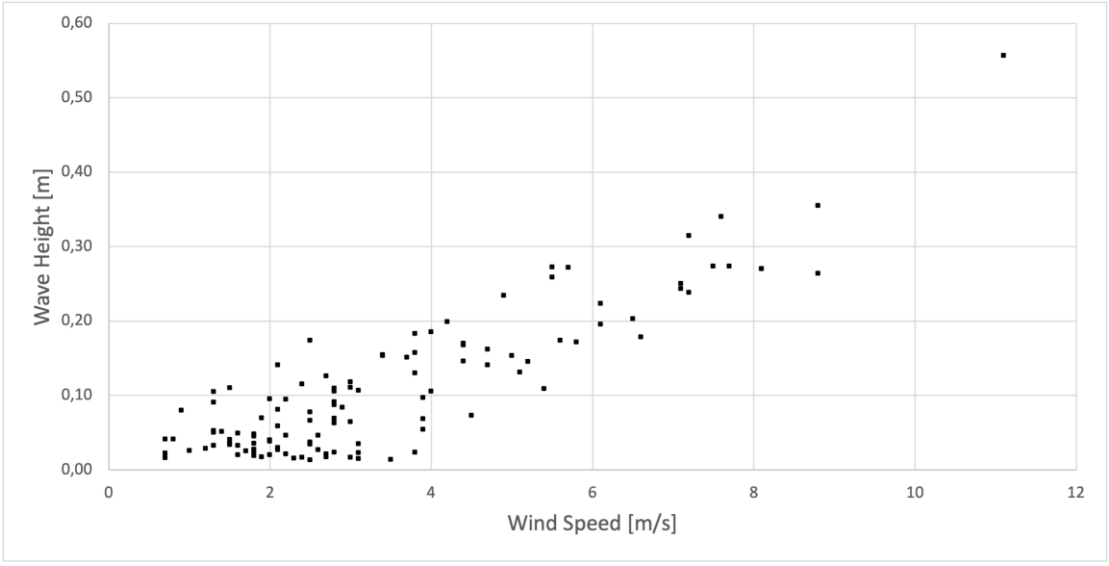

Figure 4.8 Wave height in relation to wind speed from ELJI.

The wind speed in relation to the wave direction is presented in Figure 4.9 for SMHI wind data and in Figure 4.10 for ELJI wind data. In both figures, the wave direction points are concentrated around 240° with a slightly wider spread around the lower wind speeds. Based on these graphs it does not seem to be any clear relation between the wind speed and the wave direction.

Figure 4.11 and Figure 4.12 presents the relation between the wind speed and wave period for SMHI wind data and ELJI wind data. Most wave periods are concentrated around 4 seconds for all wind speeds and hence there is no clear relation between the wind speed and wave period.

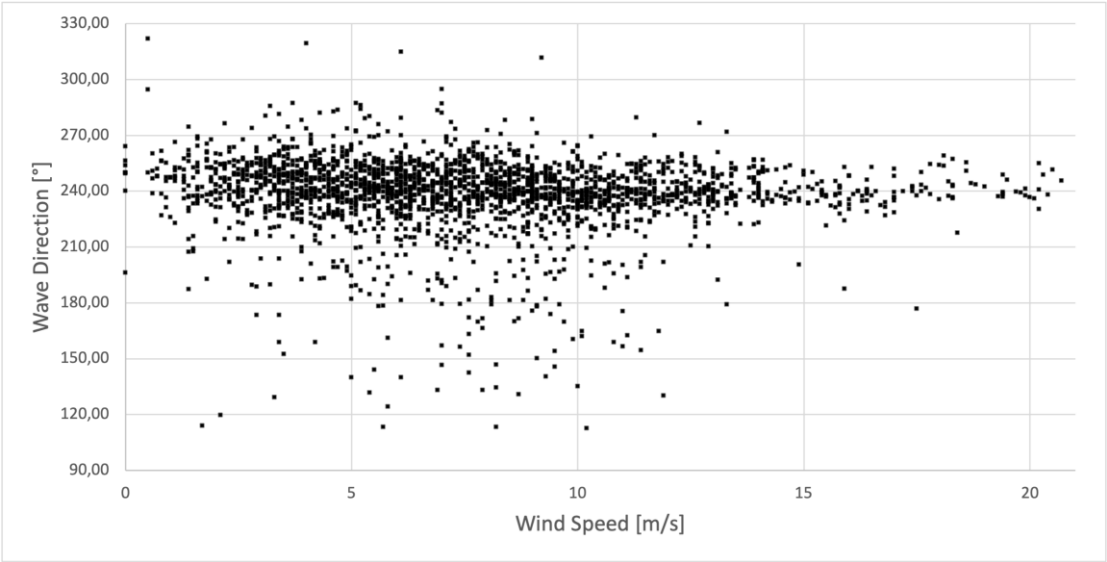

Figure 4.9 Wave direction in relation to wind speed from SMHI.

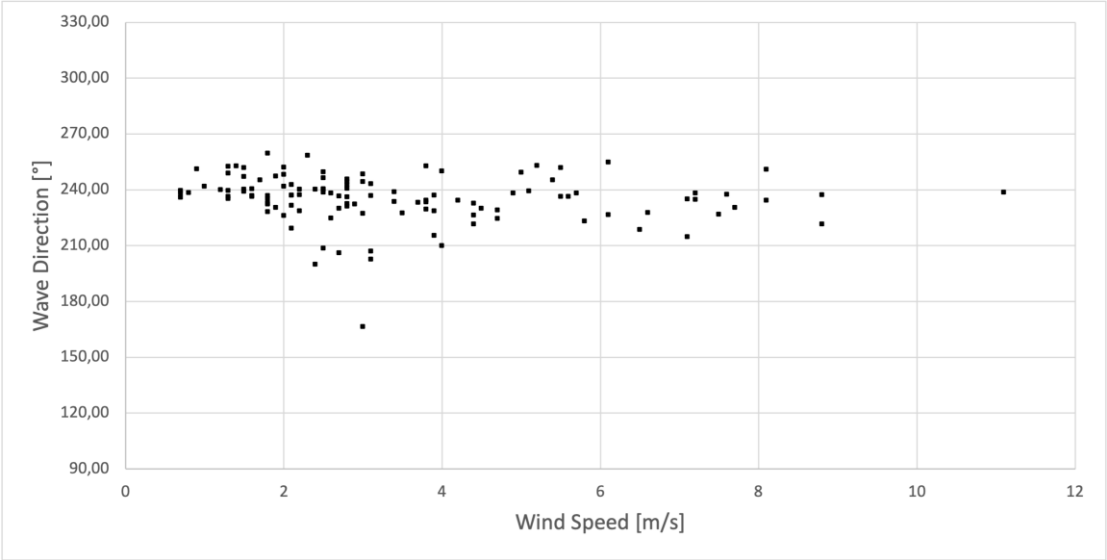

Figure 4.10 Wave direction in relation to wind speed from ELJI.

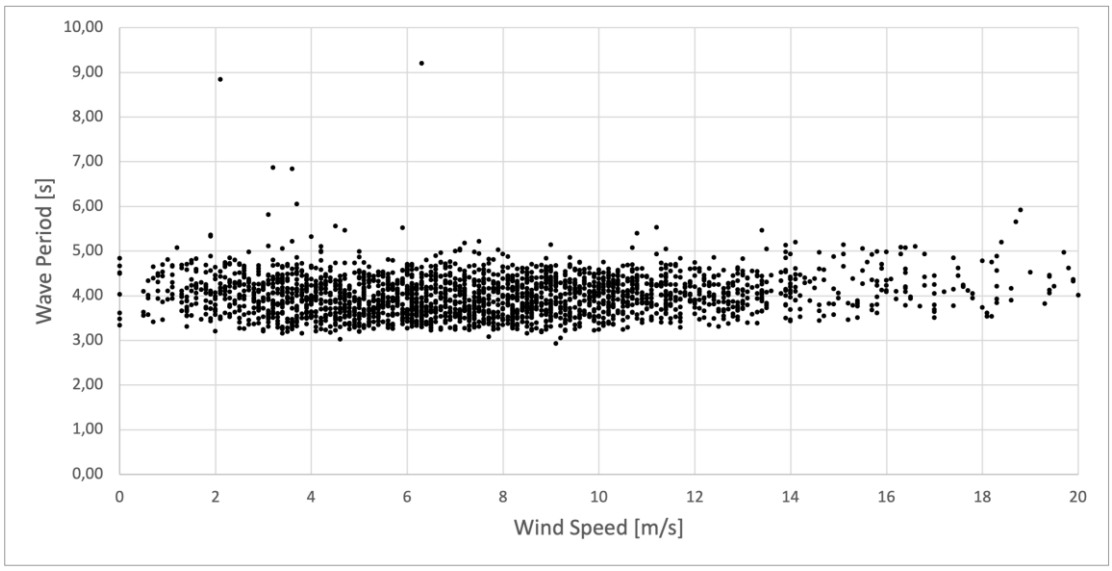

Figure 4.11 Wave period in relation to wind speed from SMHI.

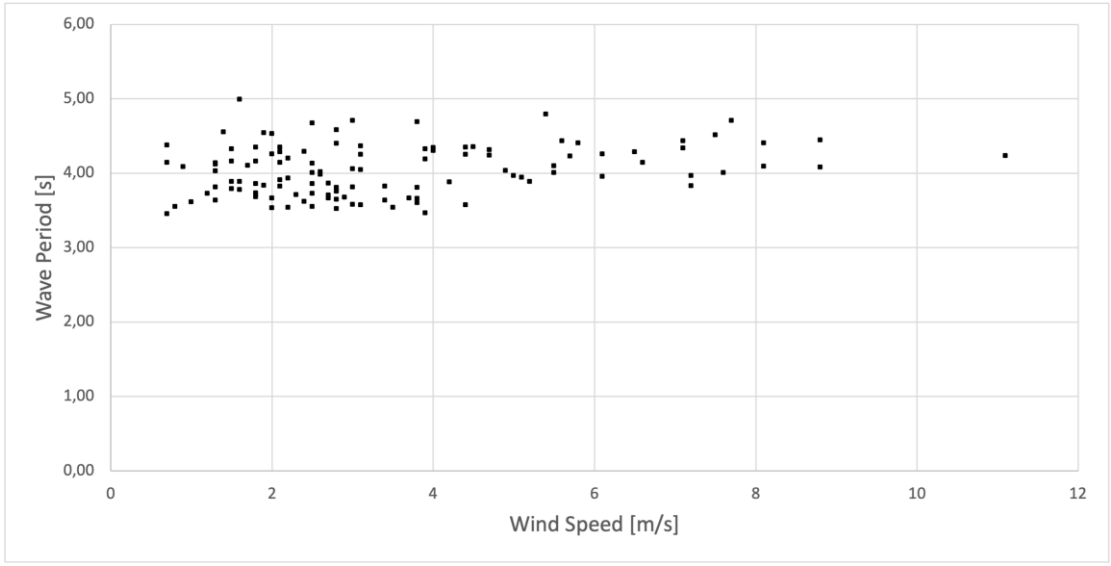

Figure 4.12 Wave period in relation to wind speed from ELJI.

At the location of the breakwater in Skärhamn, the length of the fetch varies a lot in different directions. The longest fetch is found at around 245° where the fetch is the distance between Sweden and Denmark. In theory, the highest waves should be obtained when the wind direction aligns with the direction with the largest fetch. In Figure 4.13 and Figure 4.14 the wave height is plotted against the wind direction from SMHI and ELJI. Based on these graphs the largest waves are obtained with a wind direction of around 270° which is slightly higher than expected.

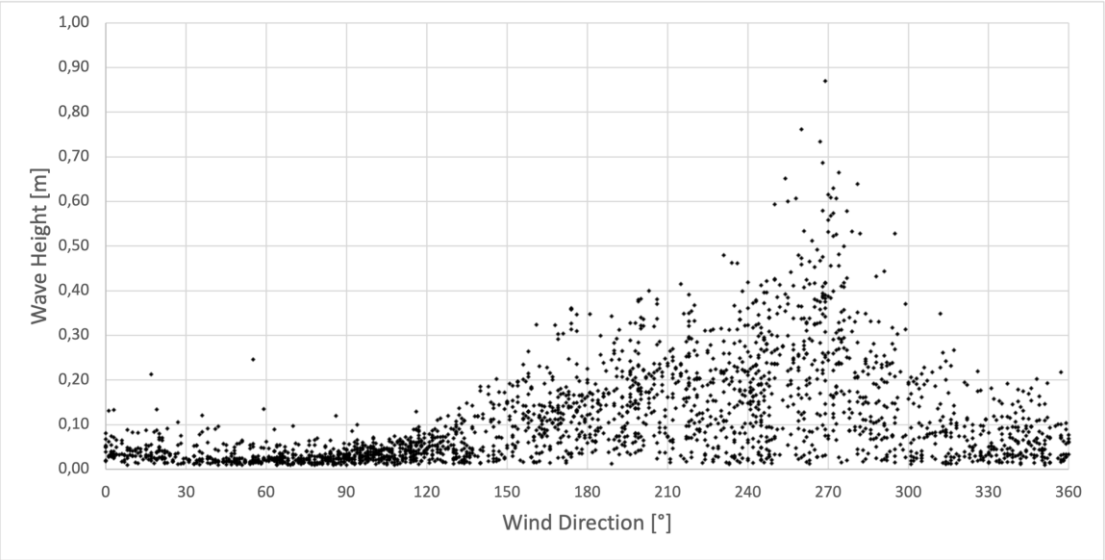

Figure 4.13 Wave height in relation to wind direction from SMHI.

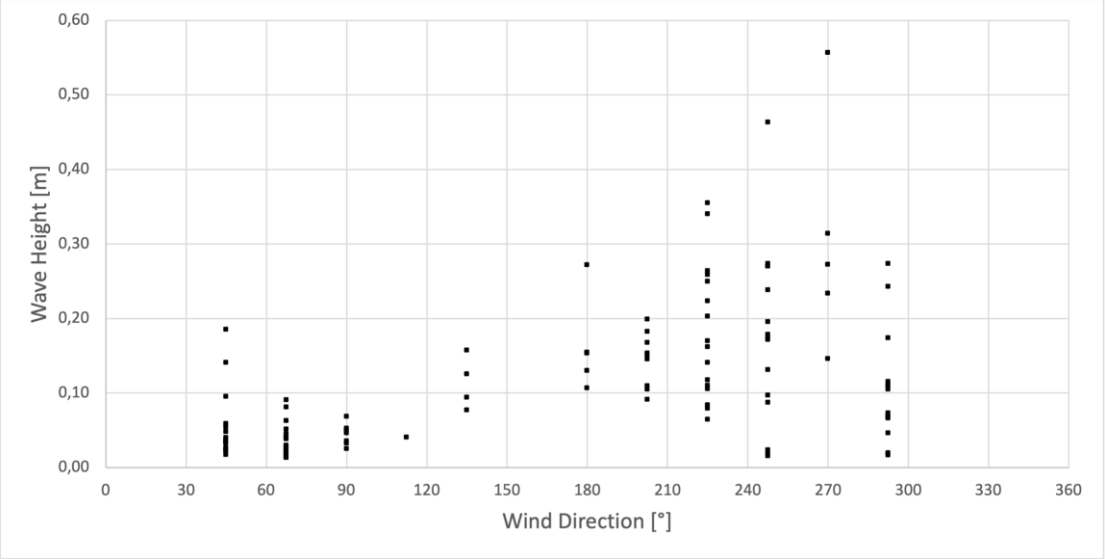

Figure 4.14 Wave height in relation to wind direction from ELJI.

Figure 4.15 and Figure 4.16 presents graphs showing the relation between wave direction and wind direction. For open water, the wave direction often aligns with the wind direction. Skärhamn is located close to shore and thus the wave pattern is affected by this. From the graphs, it is seen that the wave directions are concentrated around 240° for all wind directions.

The graphs presented in Figure 4.17 and Figure 4.18 present the wave period in relation to wind direction. Most values are concentrated around a wave period of 4 seconds at all wind directions. The longest wave periods are found around 90° which is when the wind blows from land out to sea.

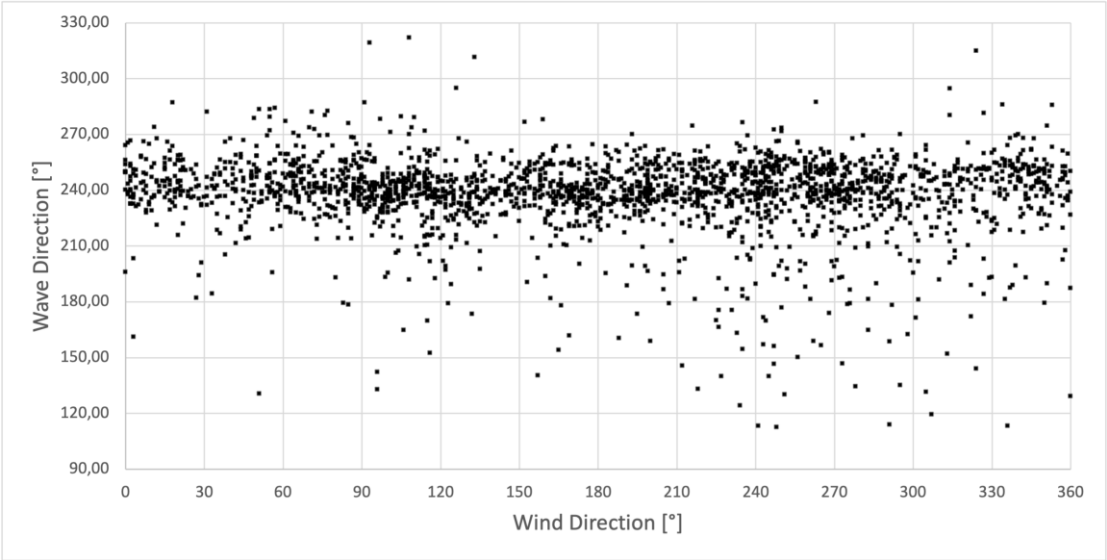

Figure 4.15 Wave direction in relation to wind direction from SMHI.

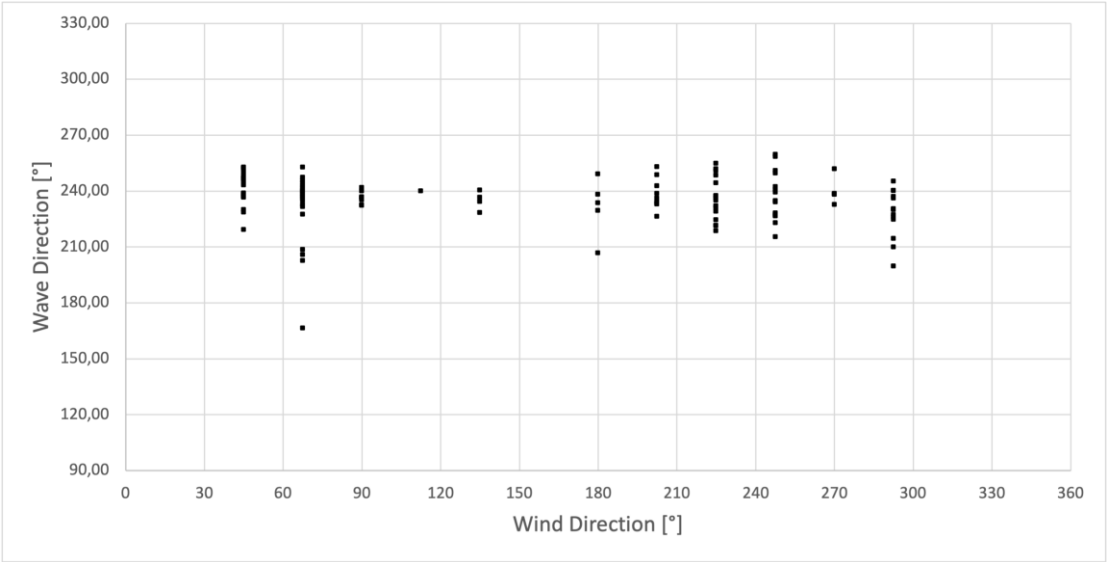

Figure 4.16 Wave direction in relation to wind direction from ELJI.

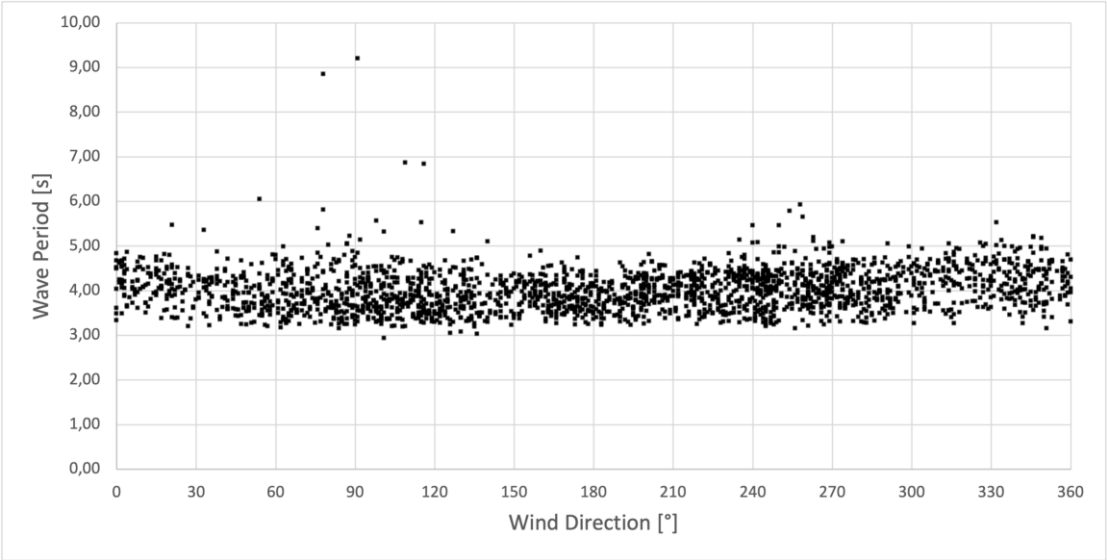

Figure 4.17 Wave period in relation to wind direction from SMHI.

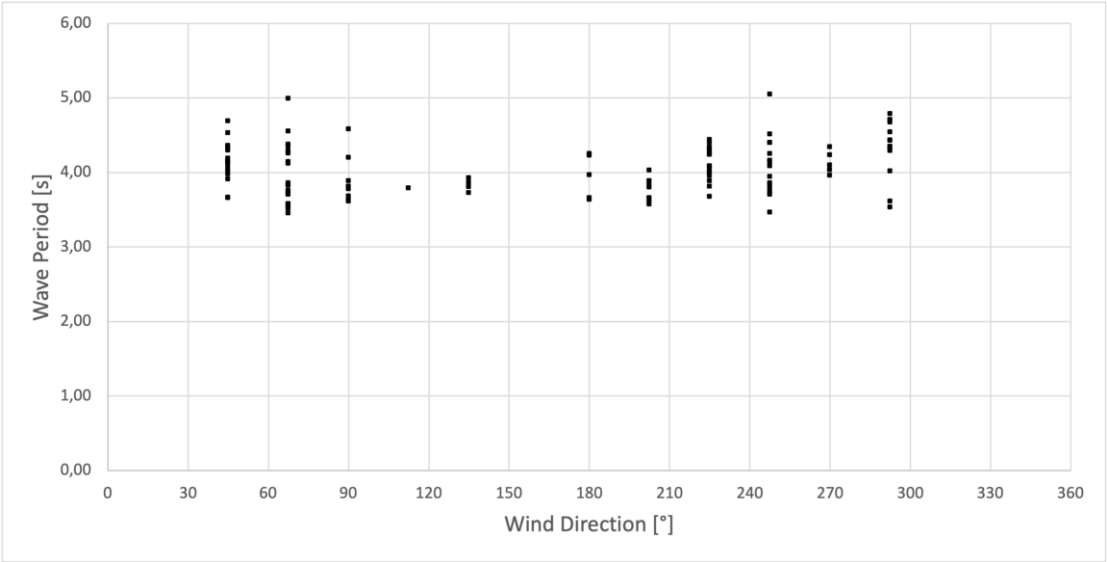

Figure 4.18 Wave period in relation to wind direction from ELJI.

4.1.4 Wavelength

The wavelength is obtained using the equations presented in Section 2.1.2 and the values presented in Table 4.3. The water depth, d, in Table 4.3 is obtained from the wave recorders. The different models in Section 2.1.2 are valid for different water depths. The valid ranges of wavelengths for the different models are presented in Table 4.4.

Table 4.3 Input variables for wavelength calculation

Parameter		Value	Unit
Gravitational acceleration	g	9.82	m/s^2
Water depth	d	9.7	m

Comparing the ranges in Table 4.4 with the results from the calculations presented in Table 4.5 gives that the Airy (Deep) model is valid up to a wave period of three seconds and that the Faltinsen model is valid for wave periods above three seconds. Due to the water depth, the models from Le Roux, Airy (shallow), and Hunt are not valid for this location.

Since the result from Faltinsen is the same as the result from Airy (Deep) at wave periods of two and three seconds, it is determined to only use the Faltinsen result for the rest of the analysis.

Table 4.4 Valid ranges of wavelengths for different models

Model	Valid range of wavelengths
Airy (Deep)	L < 19.4 m
Faltinsen	19.4 m < L < 194.0 m
Le Roux	L > 194.0 m
Airy (Shallow)	L > 194.0 m
Hunt	L > 194.0 m

Table 4.5 Result from wavelength calculation

Wavelength [m]	Wave Period [s]								
	2	3	4	5	6	7	8	9	10
Airy (Deep)	6.3	14.1	25.0	39.1	56.3	76.6	100.0	126.6	156.3
Faltinsen	6.3	14.1	24.6	36.4	48.0	59.2	70.1	80.8	91.2
Le Roux	5.3	10.0	16.0	23.4	32.2	42.4	54.1	67.3	82.0
Airy (Shallow)	19.5	29.3	39.04	48.8	58.6	68.3	78.1	87.8	97.6
Hunt	29.2	39.4	49.2	59.0	68.7	78.4	88.1	97.9	107.6

4.1.5 Wave directions

The data from the wave recorders contain measurements from waves in all different directions. When analyzing the performance of floating breakwaters, only waves in an interval around the angle normal to the breakwater are of interest. Using the compass angle from the IMU measurements, the normal direction is found to be around 226.5° with a maximum of 228.1° and a minimum of 224.3°.

The range of directions that will be included in the analysis is dependent on the location. At the location of the breakwater in Skärhamn, there are many islands between the marina and the open ocean. Based on the location and the probability shown in Figure 4.2, wave directions between 210° and 270° will be used when analyzing the breakwater performance. In the normal direction to the breakwater, this represents a range from -16.5° to 43.5°.

Figure 4.19 presents a map of Skärhamn and the islands just outside of the marina obtained from © Lantmäteriet. In the figure, a red cross is added to show where the breakwater is located since it is not visible on the original map. The two black lines show the range of wave directions that will be used in the transmission analysis.

Figure 4.19 Karta 1:10000 med fastighetsindelning 2019 [Map 1:10000 with property subdivision 2019] © Lantmäteriet.

4.1.6 Wave transmission

The wave transmission is obtained using Equation 1.1 in Section 1.1.4 with the wave data obtained from the wave recorders. Due to complications when retrieving the wave recorder located on the inside of the breakwater during the last measurement period, only data from the first and second measurement periods are used in this analysis. The wave data is filtered using the arguments explained at the beginning of Section 4.1, and the direction interval presented in Section 4.1.5.

Figure 4.20 presents the wave transmission at different wave directions. The wave directions are here relative to the normal direction of the breakwater obtained from the IMU sensor. In the scatter plot it is not possible to find any trends and thus it seems to be little to no correlation between the direction of the incoming waves and the wave transmission.

The scatter plot in Figure 4.21 presents the wave transmission in relation to the incoming significant wave height. This plot also contains too many points to see a clear relation between the incoming wave height. It is the same case for Figure 4.22 where the relation between the wave transmission and the incoming wave period is presented.

The results in Figure 4.20, Figure 4.21, and Figure 4.22 show that some of the measurements include wave transmissions above 1, meaning that the significant wave height is higher on the inside than on the outside. From the wave recorder output, it is seen that the transmission coefficient is lower than 1 for 86.3% of the time. The measurements where the significant wave height on the inside is higher than on the outside could be due to waves that have been developed on the inside of the breakwater, waves from passing boats, or waves that have been reflected on land.

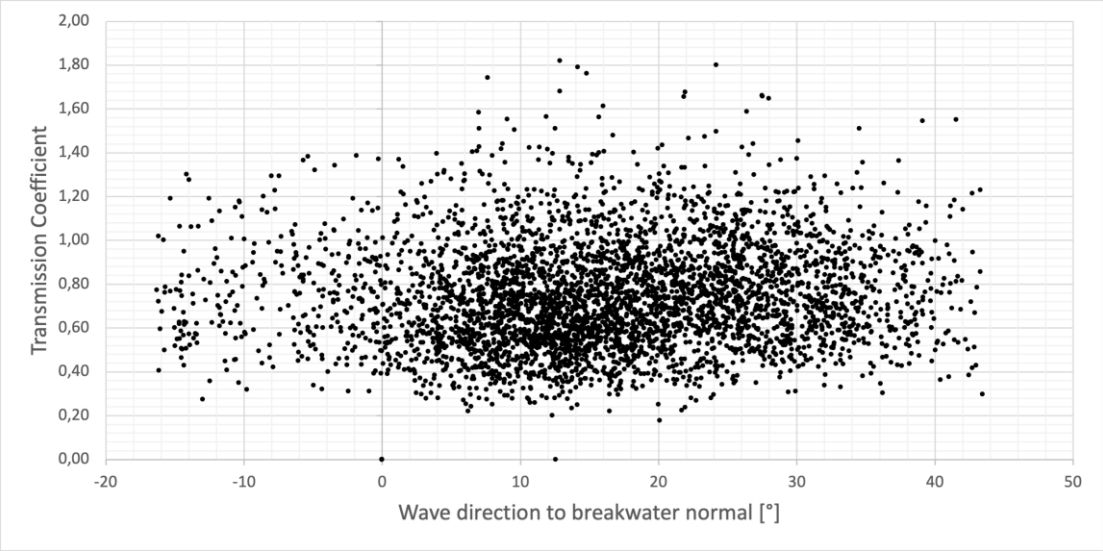

Figure 4.20 Wave transmission at different incoming wave directions.

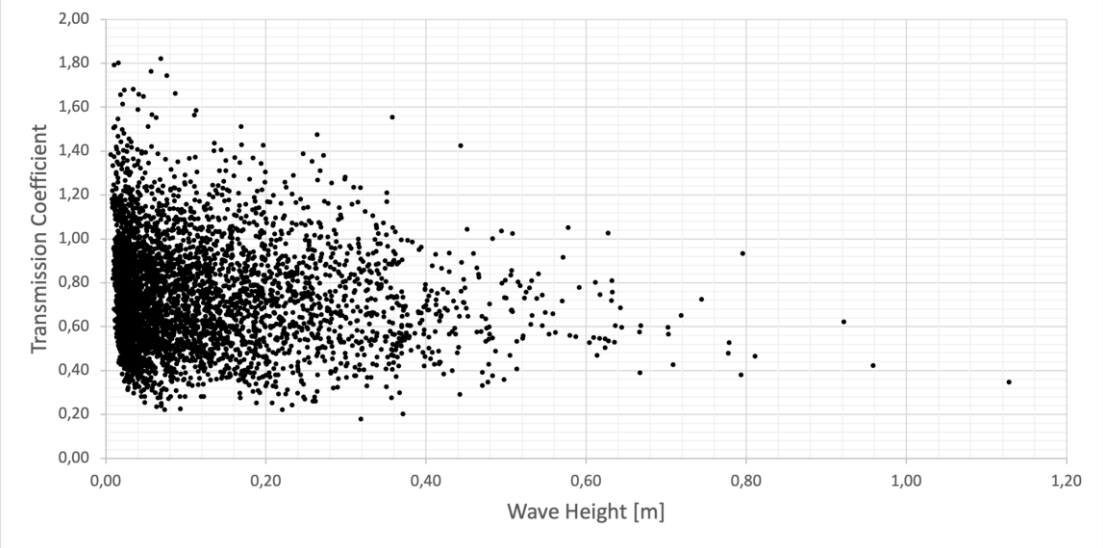

Figure 4.21 Wave transmission at different incoming significant wave heights.

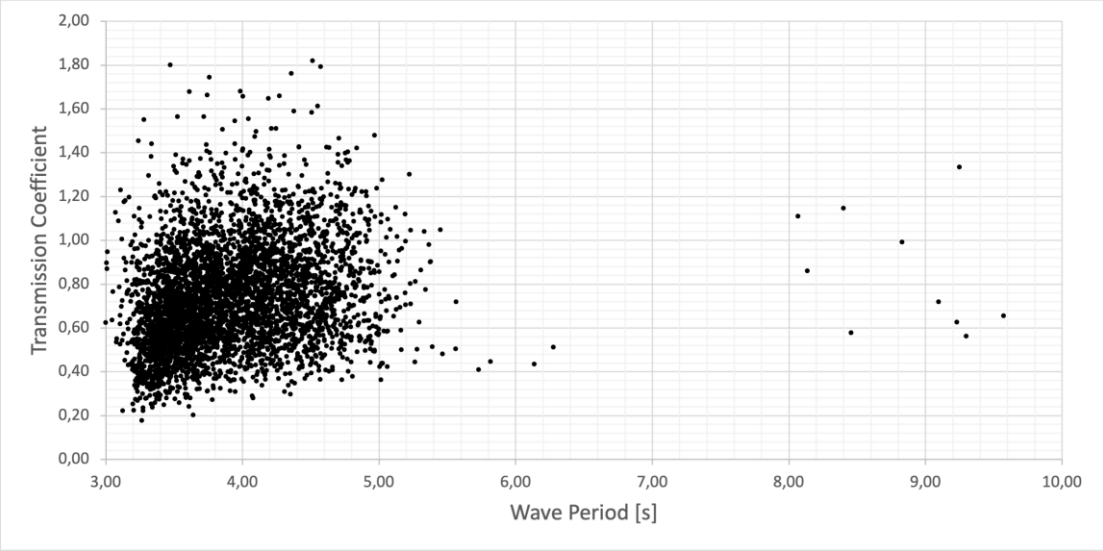

Figure 4.22 Wave transmission at different incoming mean wave periods.

The distance between the breakwater and the wave recorder on the inside (marked B in Figure 3.1) allows for waves to be created. This causes an increase in wave height on the inside which in turn increases the value of the wave transmission coefficient. To correct this the wave height increase is estimated using Equation 2.11, 2.12, or 2.13 from Section 2.1.3.

Figure 4.23 presents the estimated wave height at different wind speeds with a fetch of 15 meters and a water depth of 10 meters. Both models from Sverdrup-Munk and Bretschneider give similar estimations and since the deepwater model is less complex it is easier to only use the deepwater model. The JONSWAP equation from Hasselmann is more conservative than the equations from Sverdrup-Munk and Bredtschneider. To reduce the risk of overestimating the height increase it is decided to only use the JONSWAP equation when correcting the wave transmission.

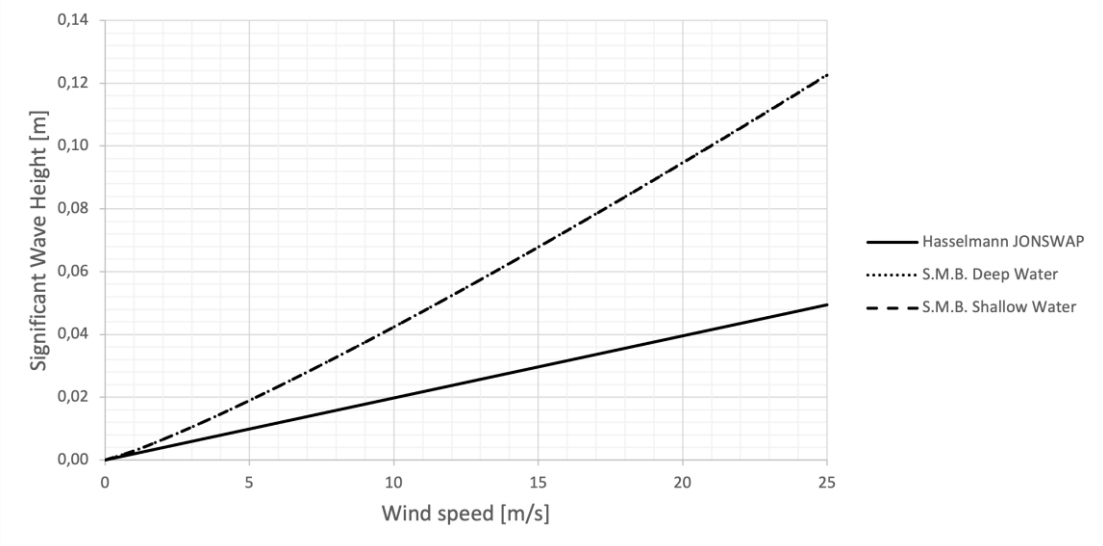

Figure 4.23 Estimated significant wave height for different wind speeds.

The wind speed is obtained as an hourly average from SMHI or as a daily average from ELJI electronics as explained in Section 3.2. To compare the wave characteristics with the wind data the wave characteristics are hourly averaged. The estimated increased wave height on the inside is calculated using the wind data from each hour and then removed from the measured wave height on the inside before calculating the wave transmission coefficient.

Figure 4.24, Figure 4.25, and Figure 4.26 present the hourly averaged wave transmission in relation to the wave direction, the incoming significant wave height, and the incoming mean wave period. Based on the scatter plot in Figure 4.24 there is no clear correlation between the wave direction and the wave transmission. The data points are scattered all over the spectrum.

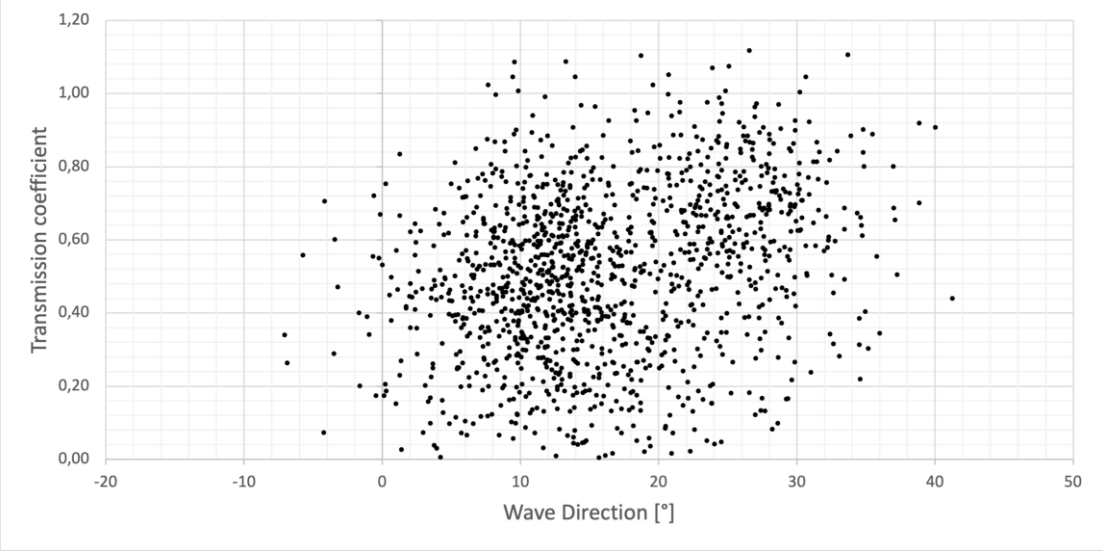

Figure 4.24 Hourly averaged wave transmission at different wave directions.

In Figure 4.25 the plot presents some correlation between the incoming significant wave height and the wave transmission. For significant wave heights below around 0.3 meters, there seems to be an increase in transmission with increased significant wave height. Above 0.3 meters, the transmission seems to decrease with an increased wave transmission.

The relation between incoming mean wave period and wave transmission, presented in Figure 4.26, shows a concentration of points around 3 to 5 seconds with the highest points located between 4 and 4.5 seconds. There is a wide spread of data points which makes it hard to draw any conclusions regarding the correlation between wave period and wave transmission.

When the data is hourly averaged it is seen that not as many data points have a wave transmission above 1. With the correction to the significant wave height on the inside, only 1.3% of the data points have a wave transmission above 1.

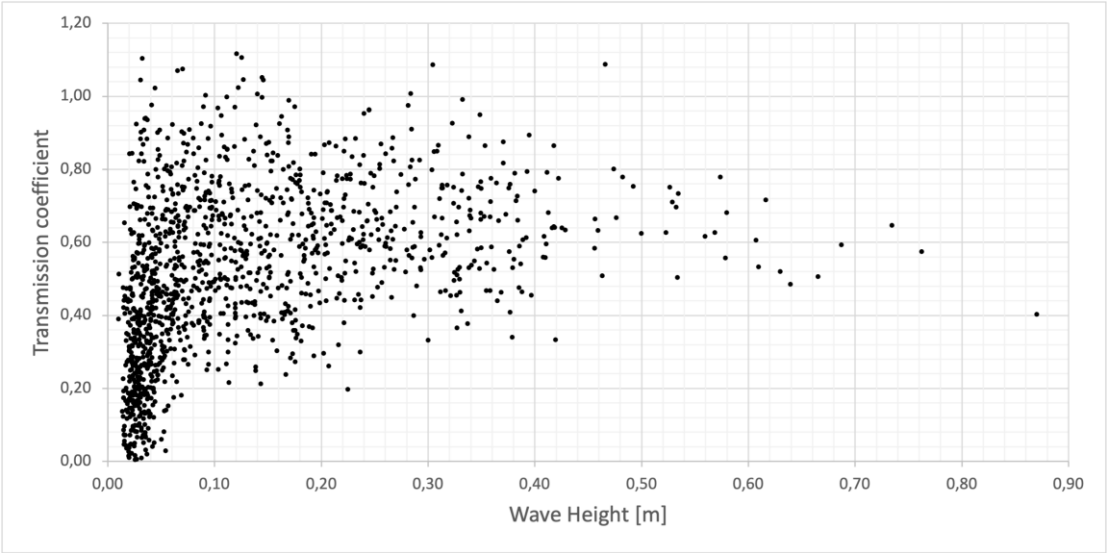

Figure 4.25 Hourly averaged wave transmission at different incoming significant wave heights.

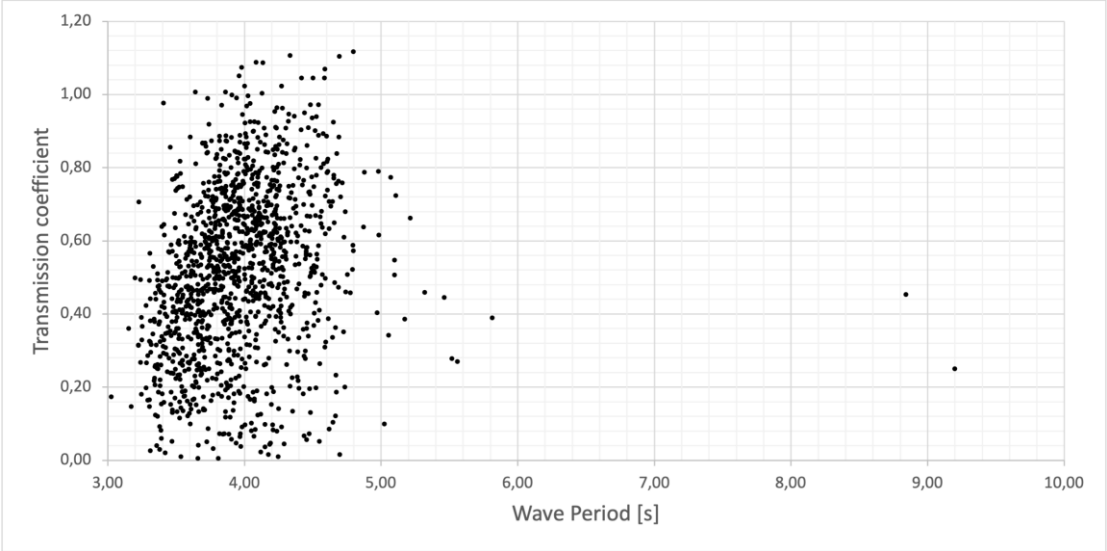

Figure 4.26 Hourly averaged wave transmission at different incoming mean wave periods.

To analyze the wave transmission using the wind data from ELJI, the wave characteristics need to be averaged for each day. The wind data from SMHI is also averaged for each day to compare the wind data from the two different sources. The station from where the ELJI wind data is measured is located closer to Skärhamn and should give a better correlation than the data from SMHI.

Figure 4.27 presents the daily averaged wave transmission at different wave directions using the wind data from both SMHI and ELJI. The points with the SMHI wind data are still very scattered and there is no clear relation between the wave direction and transmission. Using the ELJI data instead indicates that the transmission increases slightly with an increased angle between the breakwater normal and wave direction.

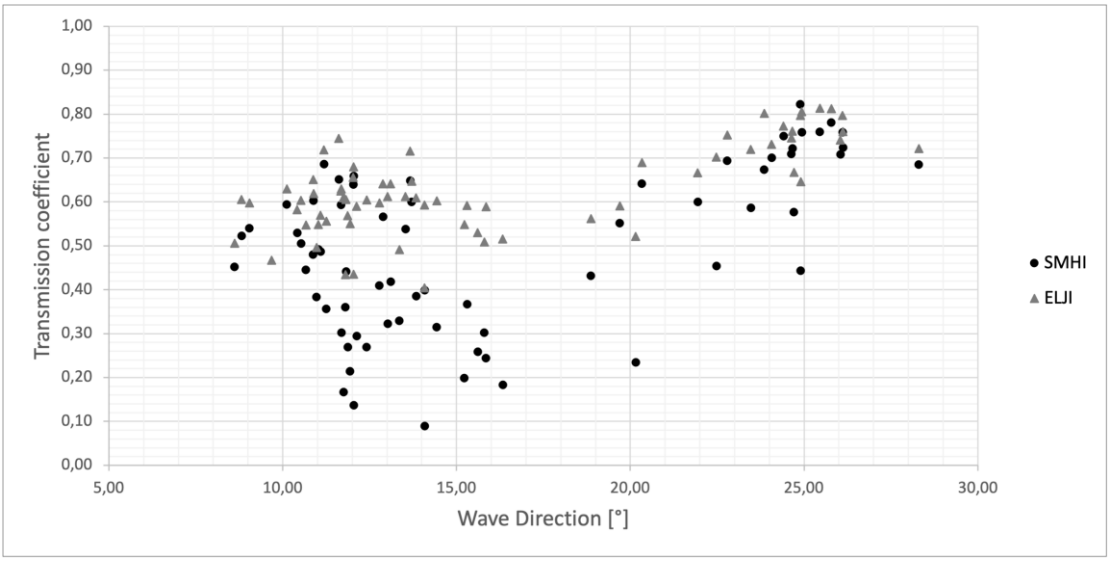

Figure 4.27 Daily average wave transmission at different wave directions.

In Figure 4.28 the daily averaged wave transmission is plotted against the incoming significant wave height. Similar to Figure 4.21 and Figure 4.25, the wave transmission increases with increased significant wave height up to about 0.3 meters and then decreases slightly with increased wave height above 0.3 meters. The increase of transmission below 0.3 meters is more drastic for the SMHI data than for the ELJI data.

Figure 4.29 presents the daily averaged wave transmission at different incoming mean wave periods for SMHI and ELJI wind data. The data points with the SMHI wind data have a large spread but there is a small trend of increased transmission for increasing wave period between 3.4 seconds and 4.6 seconds. The ELJI data points share the same trend as the SMHI trend but with a narrower spread. Both the ELJI and the SMHI have a data point at around 5 seconds where the transmission is lower than at the peak transmission at around 4.5 seconds.

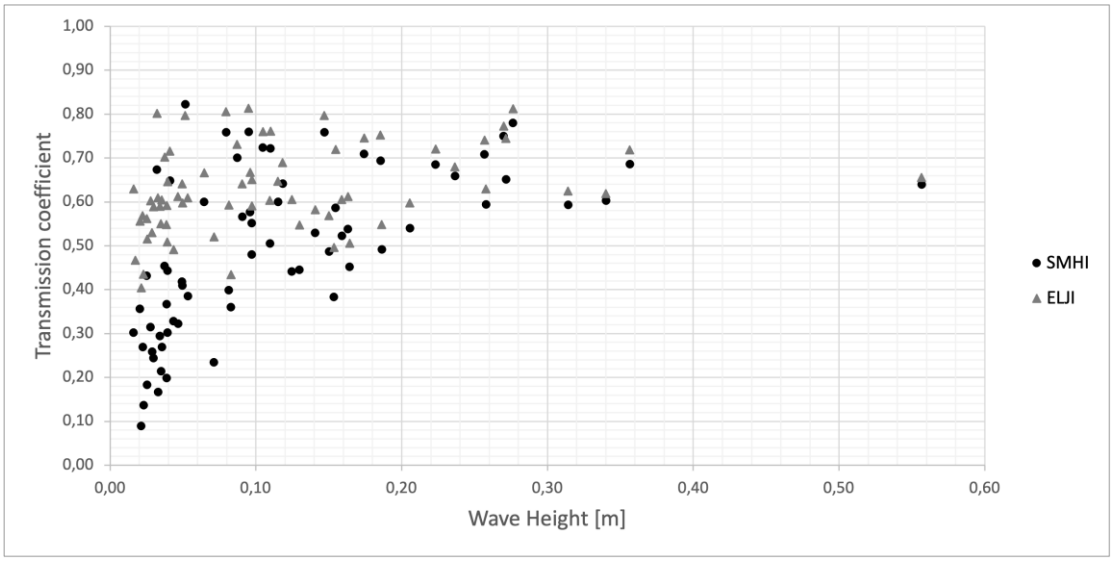

Figure 4.28 Daily average wave transmission at different incoming significant wave heights.

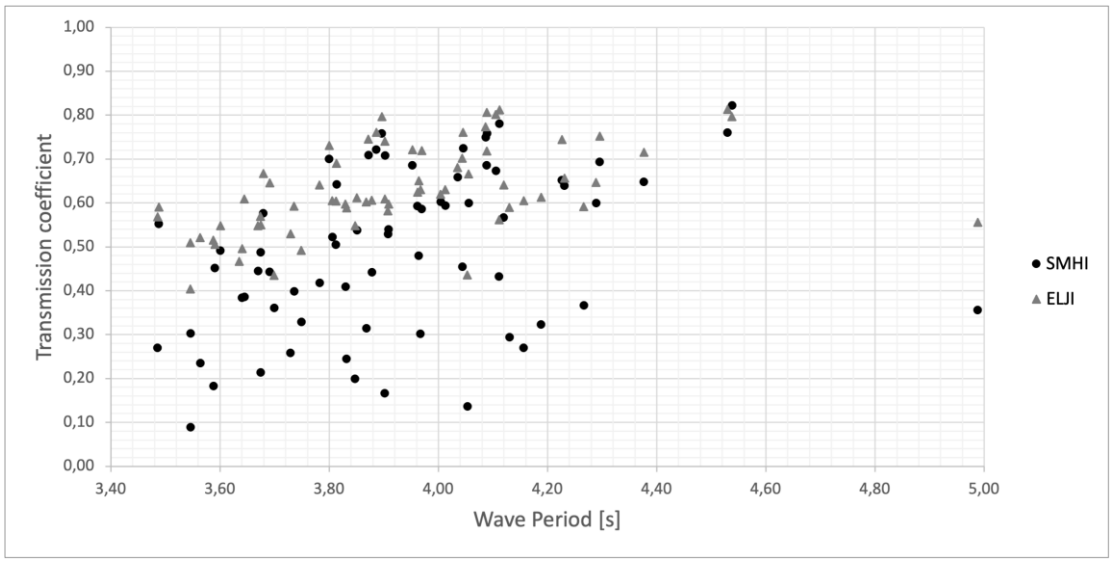

Figure 4.29 Daily average transmission at different incoming mean wave periods.

4.2 Theoretical models

The purpose of this study is to evaluate current models used to predict the performance of floating breakwaters. In Section 2.2 many different theoretical models are presented and they are divided into three groups. The first group contains models developed for vertical rigid barriers, the second group contains models developed for floating box-type breakwaters and the last group contains models developed for the Π – type breakwater that is used in Skärhamn.

The different models are dependent on different variables and this section presents the results from solving the equations in Section 2.2, using the breakwater properties in Table 1.3.

4.2.1 Vertical rigid barriers

There are two main models developed for vertical rigid barriers presented in Section 2.2.1. The first model is the Wiegel model from 1960 and since the model was developed, two corrections have been added to the model to increase the accuracy. The results of the Wiegel model and corrections are presented in Figure 4.30 for different wave periods. From the graph, it is seen that the different corrections all lower the predicted transmission coefficient and thus predict a lower transmission for the breakwater.

The Wiegel model and corrections do not include any term that is dependent on wave height and will thus estimate a constant transmission for all wave heights. The transmission is only dependent on the period of the incoming wave.

The second model in Section 2.2.1 is the Kriebel model from 2000. This model has also been updated with a correction and the result from the original Kriebel model and the corrected model is presented in Figure 4.31 for different wave periods. Since the model from Kriebel and the correction do not include any terms that are dependent on the wave height, the transmission is constant for different wave heights.

When comparing the result from the Wiegel model and corrections in Figure 4.30 with the result from the Kriebel model and correction in Figure 4.31 it is seen that the shape of the curves is similar and that the Kriebel models estimate a higher wave transmission than the Wiegel models.

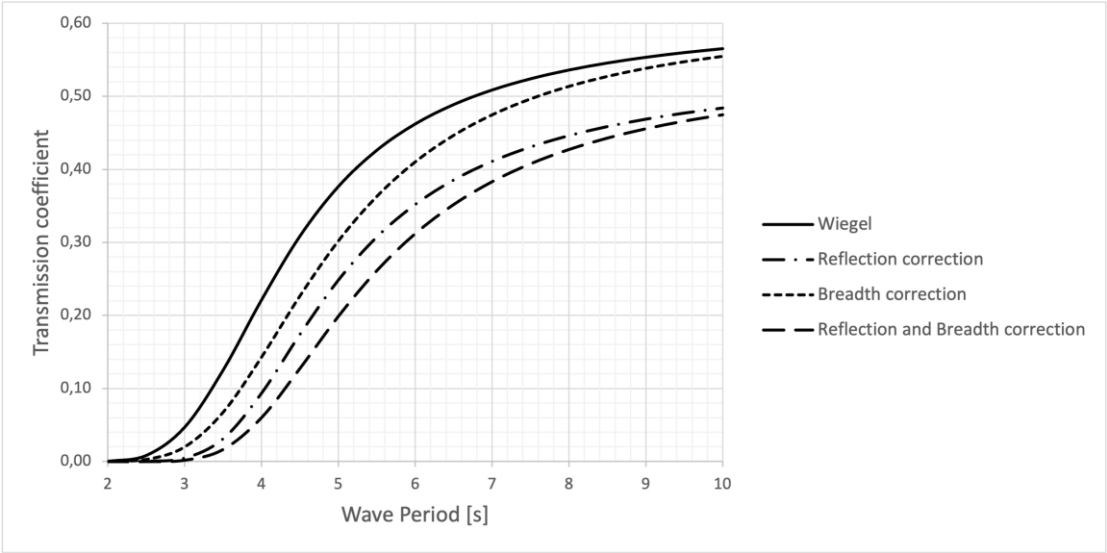

Figure 4.30 Transmission coefficient at different wave periods from Wiegel and corrections.

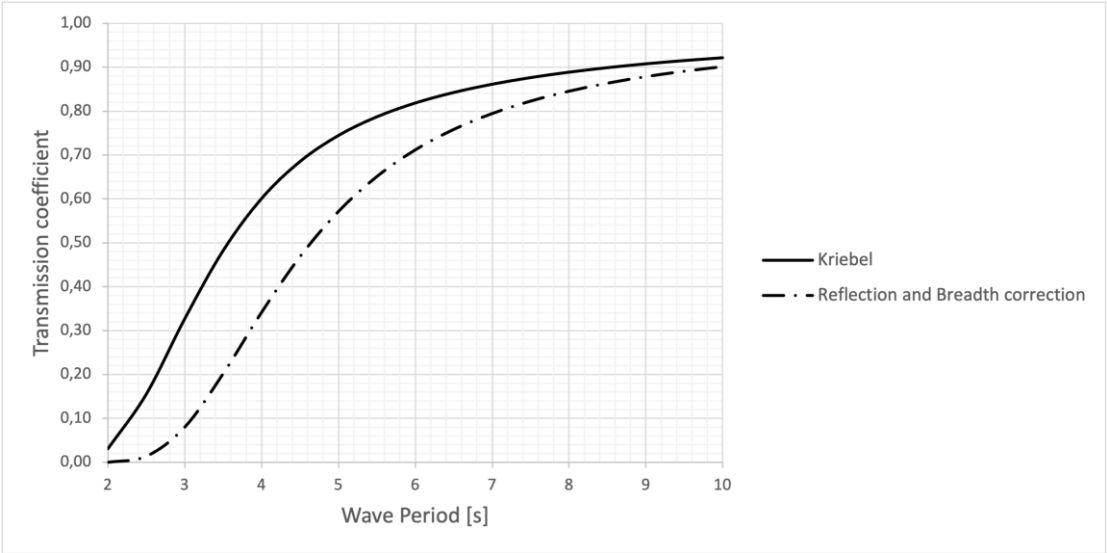

Figure 4.31 Transmission coefficient at different wave periods from Kriebel and corrections.

4.2.2 Box type floating breakwater

In Section 2.2.2, two different models developed for box-type floating breakwaters are presented. The first model was developed by Carr in 1951 and the second model was developed by Macagno in 1953. The results of these models are presented in Figure 4.32 for different wave periods. Since neither of the models include a variable that is dependent on the wave height, both models will be constant for different incoming wave heights.

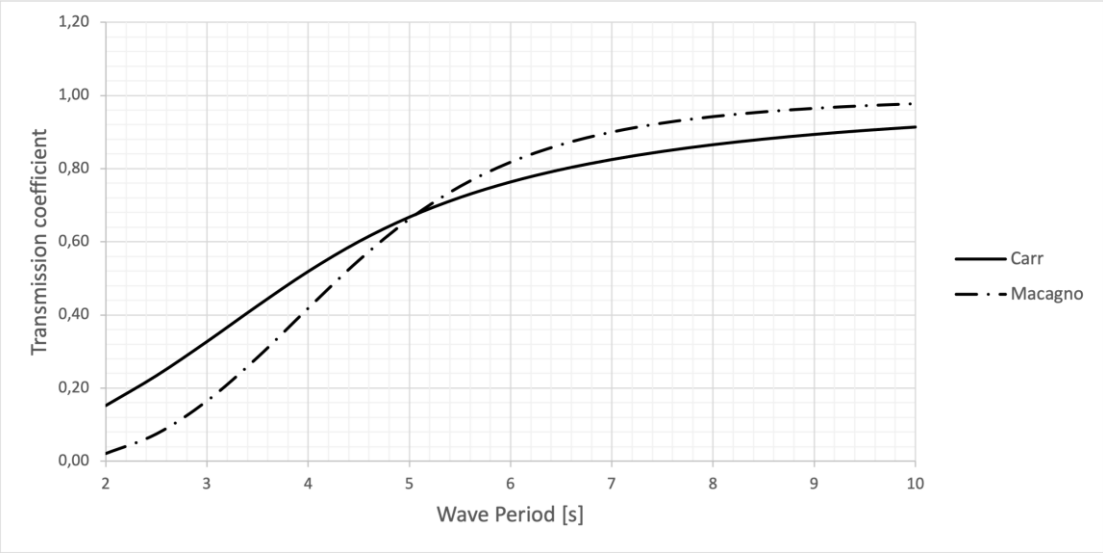

Figure 4.32 Transmission coefficient at different wave periods from Carr and Macagno.

4.2.3 Π - type floating breakwater

Section 2.2.3 presents three models that are developed for Π – type breakwaters, the same type as the one located in Skärhamn. The first model is a model from Ruol et al. from 2013 that is a modification to the Macagno model developed for box-type breakwaters. The results from these three models are presented in Figure 4.33 for different wave periods.

The shape of these models varies slightly from the previous models and the model from Ruol et al. has a local maximum at a wave period of around 4.5 seconds and then it decreases slightly before increasing again. The model from Günaydin and Kebdaşli estimates the lowest transmission coefficient of all models at the higher wave periods. Moghim and Botshekan's model is the only model that increases throughout the whole wave period spectra.

Similar to the previous models, the model from Ruol et al., is constant for all wave heights since it does not include a variable that is dependent on the wave height. The models from Günaydin and Kebdaşli, and Moghim and Botchekan include the wave height in the model and are thus dependent on the wave height which can be seen in Figure 4.34. The graph in Figure 4.34 shows that the model from Günaydin and Kebdaşli predicts an increased wave transmission for increasing wave height and that the model from Moghim and Botshekan predicts a decreased wave transmission for increasing wave heights.

In Figure 4.33 the transmission coefficient from the Günaydin and Kebdaşli model and the Moghim and Botshekan model is an average over the wave heights and similarly, the transmission coefficients of the models in Figure 4.34 are an average over the wave periods.

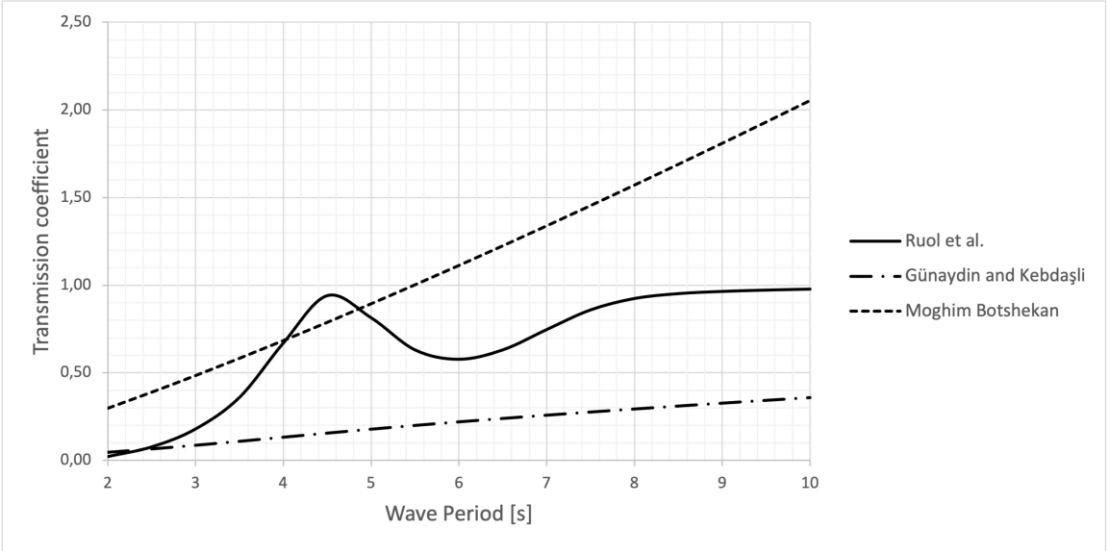

Figure 4.33 Transmission coefficient at different wave periods from Ruol et al., Günaydin and Kebdaşli, and Moghim and Botshekan.

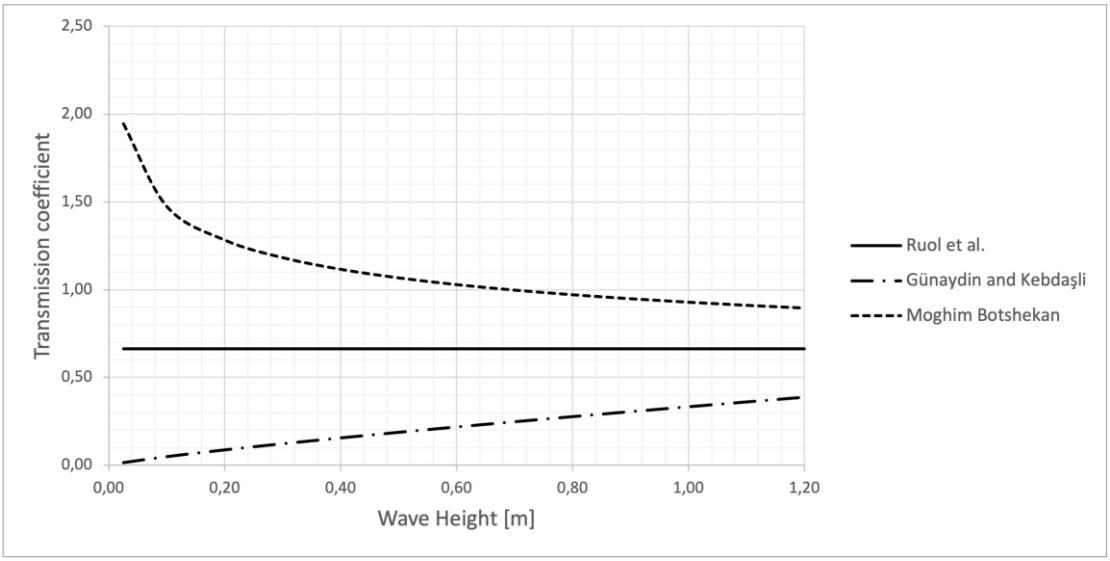

Figure 4.34 Transmission coefficient at different wave heights from Ruol et al., Günaydin and Kebdaşli, and Moghim and Botshekan.

4.3 Ansys AQWA result

In Section 3.4, Ansys AQWA was presented as a tool that could be used to evaluate the performance of floating breakwaters. Figure 4.35 presents the transmission coefficient at different wave periods after using the field point approach as explained in Section 3.4.

In the graph, a local maximum is seen at a wave period of around 4 seconds where the transmission coefficient reaches a value of about 1.2. This indicates that at a wave period of 4 seconds the waves on the inside should be 1.2 times the height of the incoming waves. The simulation in Ansys AQWA does not include any anchoring which could be what causes the peak at the wave period of four seconds. With anchoring, the movement of the breakwater would be dampened which could reduce the magnitude of this peak.

When the Ansys AQWA results are compared with the result of the theoretical models it is seen that Ansys AQWA in general estimates a lower transmission than the theoretical models except for the peak at four seconds. The result obtained using the field points approach is only dependent on the wave period and is constant for all incoming wave heights.

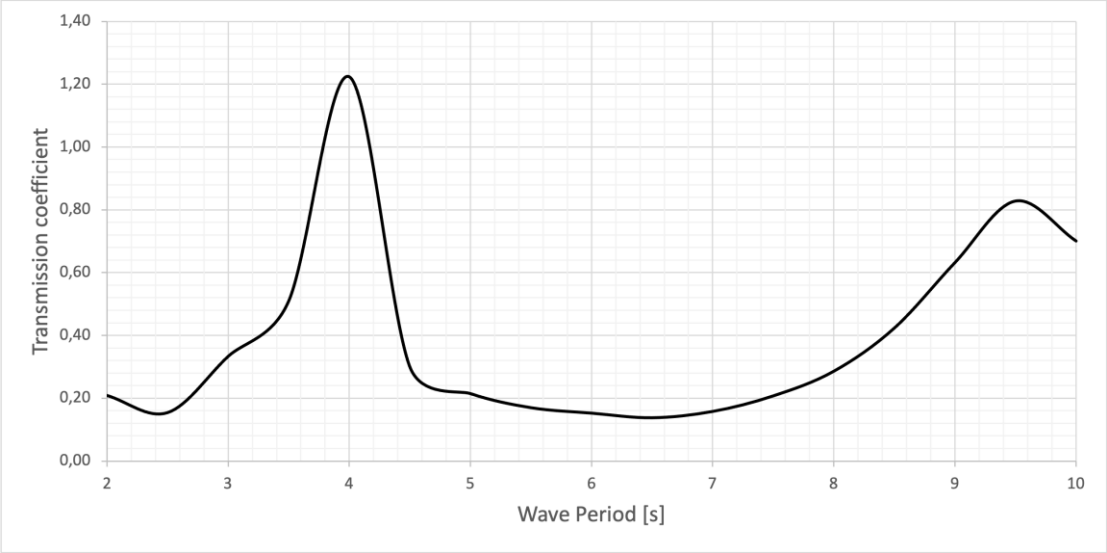

Figure 4.35 Transmission coefficient at different wave periods from Ansys AQWA.

4.4 Breakwater movement

These breakwater movement results are based on IMU readings between the 23rd of February 2021 to the 2nd of March 2021 and between the 23rd of March 2021 and the 18th of April 2021. Since the wave recorder placed on the inside was not obtained after the last measurement, it is only possible to analyze the correlation between transmission and movement during the measurement at the end of February.

4.4.1 Wave characteristics and breakwater movement

When comparing the hourly average of wave characteristics (height, period, and direction) with the movement of the breakwater, a parameter called max angle will be used. Max angle is the highest measured angle during every hour.

Figure 4.36 and Figure 4.37 presents the highest measured roll and pitch angle during one hour in relation to the incoming significant wave height during the same hour. The roll and pitch angle increases with an increased significant wave height with some spread around the mean. It is seen that the roll angle increases more rapidly but contains more spread than the pitch angle.

The relation between roll and pitch angle and the wave period is presented in Figure 4.38 and Figure 4.39. The roll seems to increase up to 4 seconds and then decrease slightly to 4.75 seconds before lastly increasing slightly. The graph presenting the pitch angle instead increases slightly through the whole spectrum of wave periods presented in the graph.

The direction of the waves does not have a clear relation to the roll and pitch angle which can be seen in Figure 4.40 and Figure 4.41. In these graphs, there is a wide spread within the graph with only a larger concentration of points at the most common wave direction.

How the transmission coefficient is affected by the movement of the breakwater can only be analyzed using the data from the 23rd of February until the 2nd of March 2021. This is a very short period and does not contain that many data points. However, it indicates if there is a relation between breakwater movement and transmission or not.

In Figure 4.42 and Figure 4.43, the relation between the transmission coefficient and the highest measured roll and pitch angle is presented. It is seen that the transmission is increased, both for an increased roll angle and an increased pitch angle.

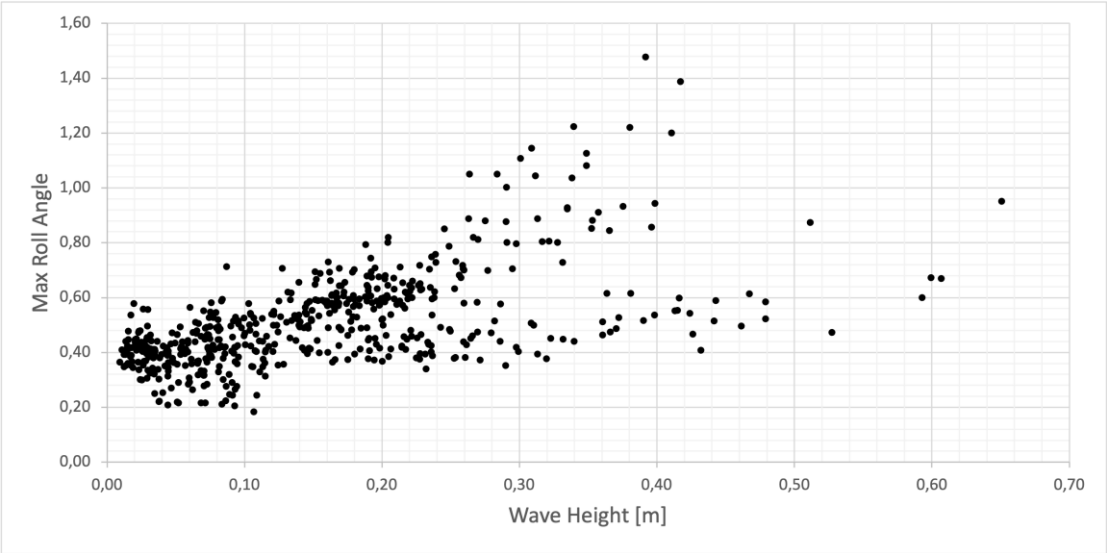

Figure 4.36 Maximum roll angle in relation to incoming significant wave height.

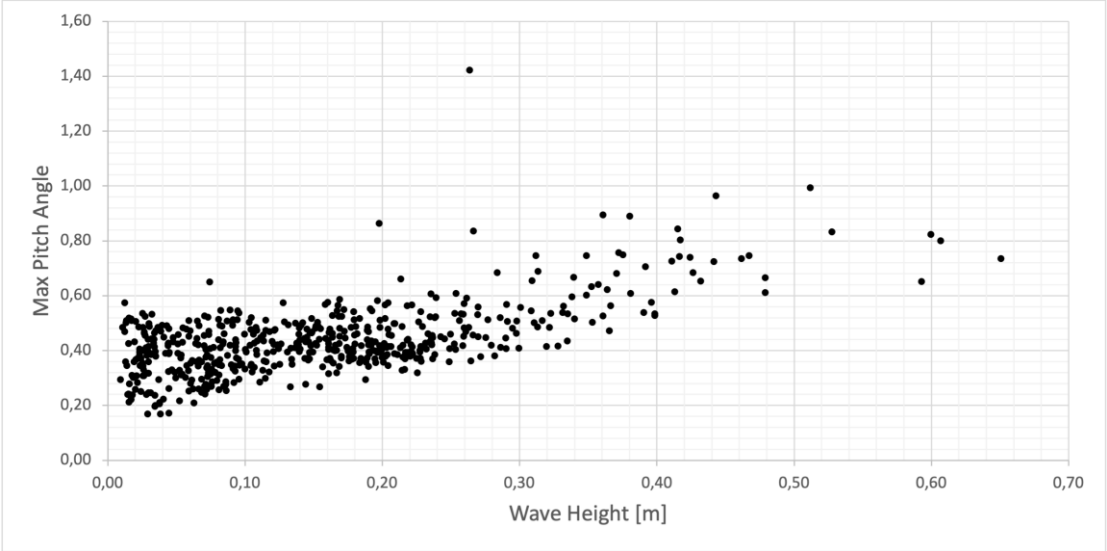

Figure 4.37 Maximum pitch angle in relation to incoming significant wave height.

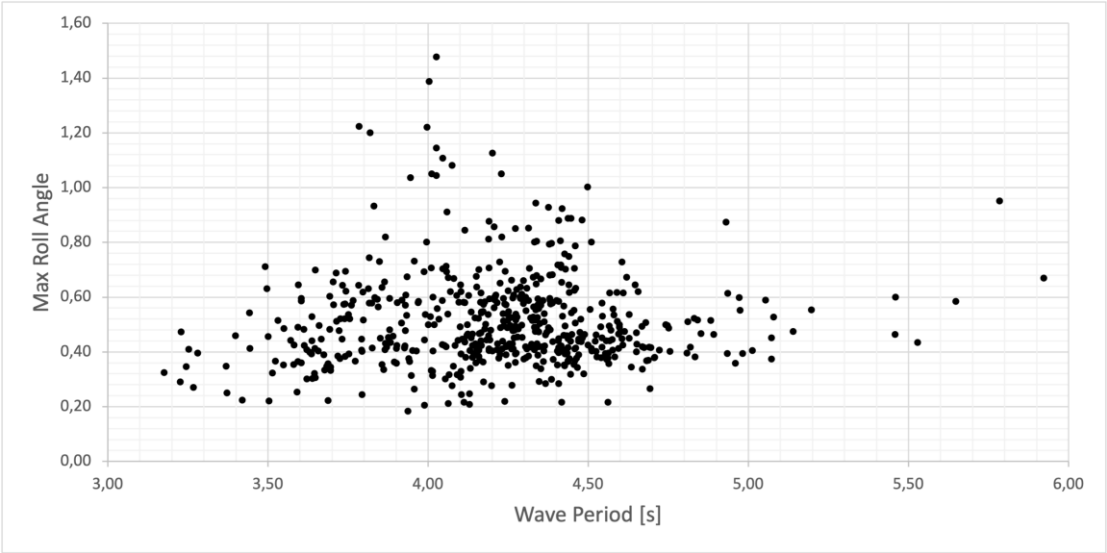

Figure 4.38 Maximum roll angle in relation to incoming mean wave period.

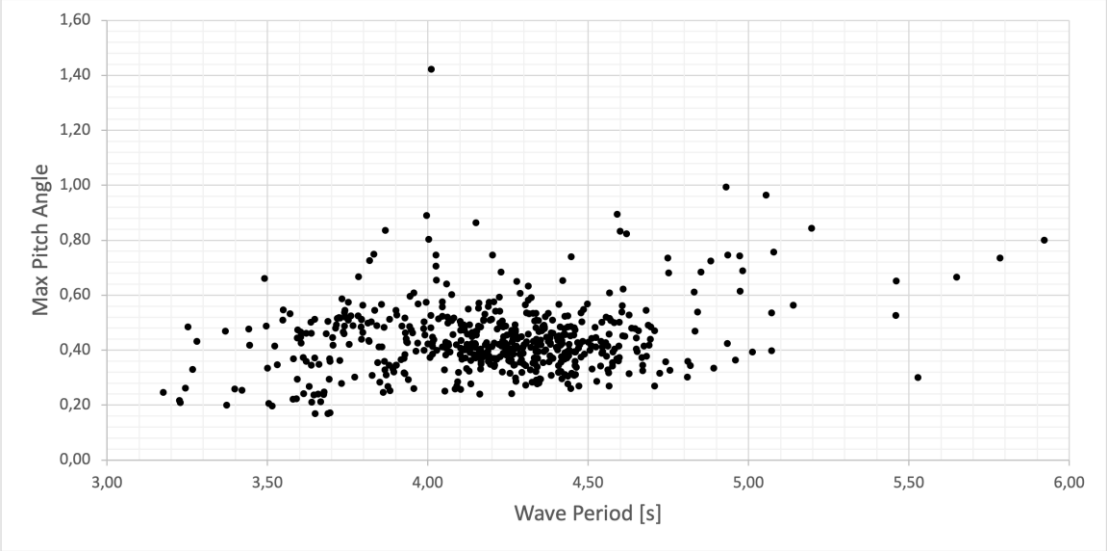

Figure 4.39 Maximum pitch angle in relation to incoming mean wave period.

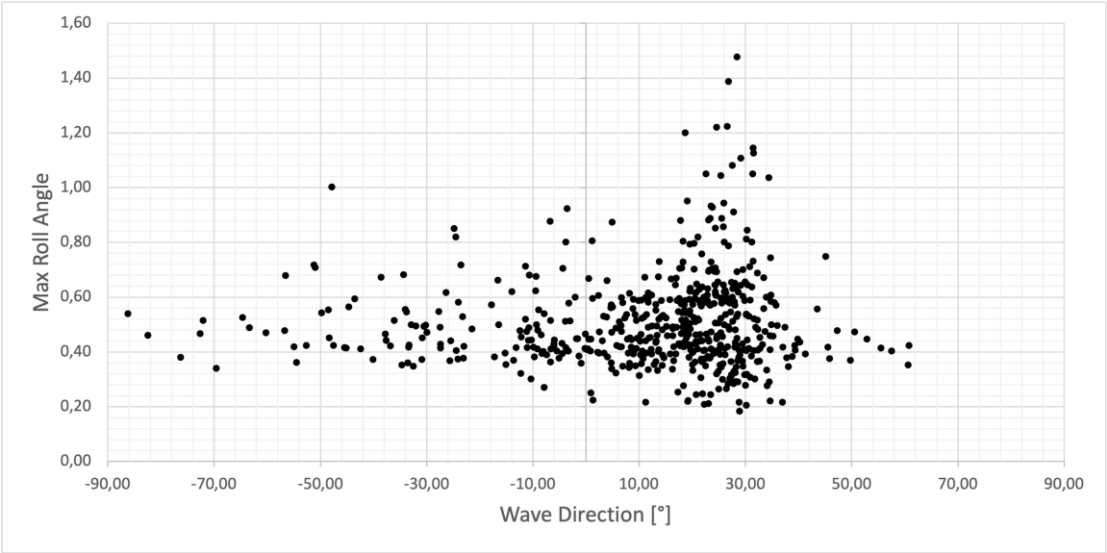

Figure 4.40 Maximum roll angle in relation to the wave direction.

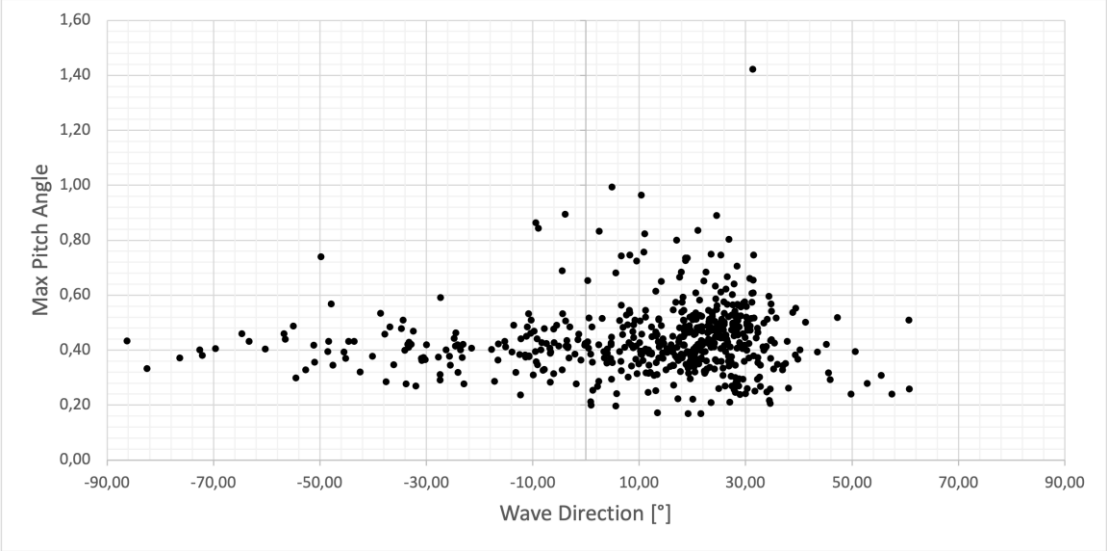

Figure 4.41 Maximum pitch angle in relation to the wave direction.

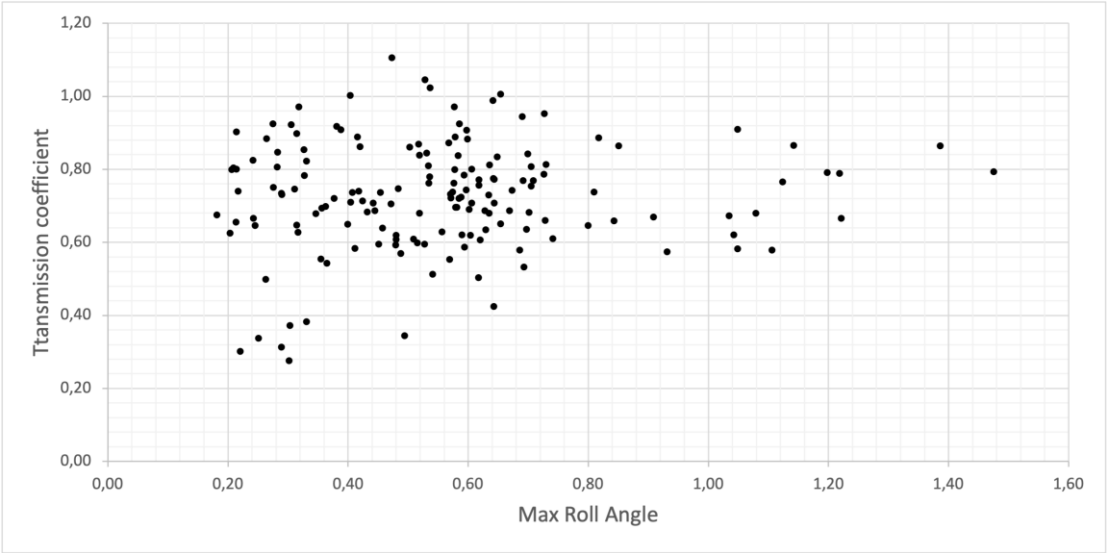

Figure 4.42 Transmission coefficient at different roll angles.

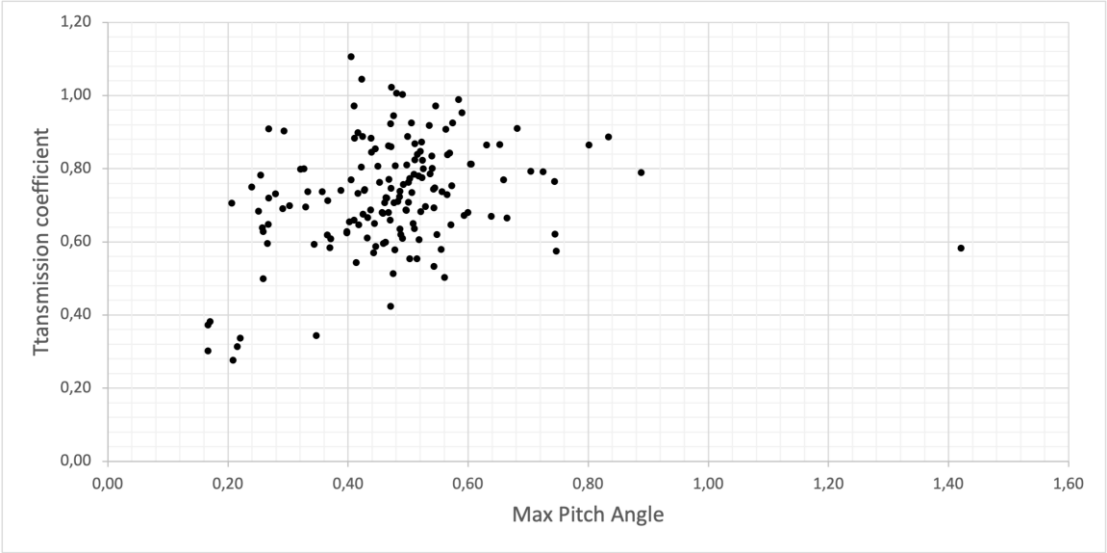

Figure 4.43 Transmission at different pitch angles.

4.4.2 Strip theory

A floating breakwater fits well within the assumptions made for strip theory presented in Section 2.3.1. For this application, strip theory is not suitable since the method is only developed for analyzing the movement of a structure based on an incoming wave, and not how a wave transmits through the structure. For that reason, it was decided not to further investigate the possibility of using strip theory for analyzing the breakwater performance.

4.4.3 Natural roll period

The natural roll period of the breakwater is calculated using Equation 2.35 with the mass and moment of inertia presented in Table 1.3. When running the Ansys AQWA simulation the metacentric height is estimated to 7.2 meters for roll motions and 30.5 meters for pitch motions.

The results from the calculation are presented in Table 4.6, however, these values do not take into account the anchoring chains or connections between breakwaters. The anchoring chains and connections will resist movement and thus affect the natural roll frequency of the system. If the anchoring and connections were to be added it would most likely increase the natural period of both roll and pitch motions.

Table 4.6 Result of natural roll period calculation for roll and pitch motion

Motion	Period
Roll	2.33 s
Pitch	2.06 s

5 Discussion

This section compares the different results presented in Section 4 to make conclusions regarding relations between wave climate and wave transmission. The results from the different estimation methods presented in Sections 4.2 and 4.3 are compared with the measured transmission presented in Section 4.1.6, to find the most suitable estimation method.

The motion analysis presented in Section 4.4 is discussed to find relations between breakwater movement and wave transmission. Throughout the section, sources of error are discussed as well as future investigations.

5.1 Wave climate and transmission

The data from the wave recorders have a wide spread and it is hard to see any correlation between the wave climate and the wave transmission. By first averaging the data hourly and then daily it is possible to find some trends for wave height and wave period.

Analyzing Figure 4.24 to Figure 4.29 gives that the wave transmission is most dependent on the incoming wave period. There is quite a bit of spread in all figures but there seems to be a peak in transmission around a wave period of 4.5 seconds and the transmission seems to decrease slightly with an increased wave height. The decrease of transmission with increased wave height is more clear in the hourly average in Figure 4.25 and for the daily average in Figure 4.28 there instead appears to be a peak of transmission at 0.3 meters.

During the first measurement period, the wave recorders were not synchronized in time which means that the wave climate on the inside and outside was measured with a 10-minute time gap. This should not cause that big of an error since the wave climate does not change much in 10 minutes.

Another possible source of error is the short sample time during the first two measurement periods. From Table 3.1 it is seen that the sample time was 64 seconds for the first two measurement periods. With a mean wave period of 3.96 seconds, this means that only about 16 waves were used to determine the significant wave height and mean wave period. If more waves were included in the sample, a more accurate estimation of the significant wave height and mean period would have been obtained. This was corrected before the last measurement but since the wave recorder on the inside was not obtained after the last measurement it is not included in the transmission analysis. The new settings used during the last measurement meant that about 260 waves would have been included instead.

When estimating the increased wave height on the inside of the breakwater, the JONSWAP equation was used with a fetch of 15 meters. When doing the correction, the wind direction was not taken into account and since the fetch varies depending on the direction of the wind, so should the correction have done. This is a source of error that could affect the final result slightly.

5.2 Theoretical transmission and measured transmission

To determine which theoretical model that is best suited for evaluating the performance of the SFBW1000(3.0) breakwater, the results from the theoretical models are compared to the measured transmission from the wave recorders. In Figure 5.1 to Figure 5.4, the wave transmission corrected using the JONSWAP equation and ELJI wind data are plotted together with the result from the theoretical models. Based on these graphs it is seen that the best suiting models are the Kriebel model, the Ruol et al. model, and the Moghim and Botshekan model.

In Figure 5.5, the theoretical Π-type models are plotted together with the corrected transmission from Figure 4.28 for different wave heights. This graph shows that the Moghim and Botshekan model tends to overestimate the wave transmission while the Ruol et al. model estimates the transmission very close to the measured value for all wave heights. Due to this, the Ruol et al. model is assumed to be better suited than the Moghim and Botshekan.

Figure 5.6 presents the Ansys AQWA result together with the measured transmission. The Ansys AQWA result does not fit well with the measured result and thus it is not considered to be a suitable model to use when estimating the performance. Ansys AQWA is a powerful tool with many different settings and thus it is possible that with other settings a better suiting result would be obtained. Though, since the complexity of the AQWA software is much higher than any of the other estimation methods, the other methods are considered more suitable for this application.

This leaves two models that are considered to be the best suiting models, the Kriebel model, and the Ruol et al. model. The difference between the two models is that the Kriebel model does not include the local peak at around 4.5 seconds. The daily average of the measured data gives a small indication that there is a local maximum at around 4.5 seconds since there is a data point at 5 seconds where the transmission is lower than at 4.5 seconds. There are, however, too few data points above 4.5 seconds to confidently draw this conclusion.

The conclusion that can be drawn from this study is that the Ruol et al. model and the Kriebel model are the two most suitable models. Further studies are recommended to accurately determine the most suitable model. In these future studies, the wave transmission should be measured at different locations, with different breakwaters and anchoring systems to find the most suitable model.

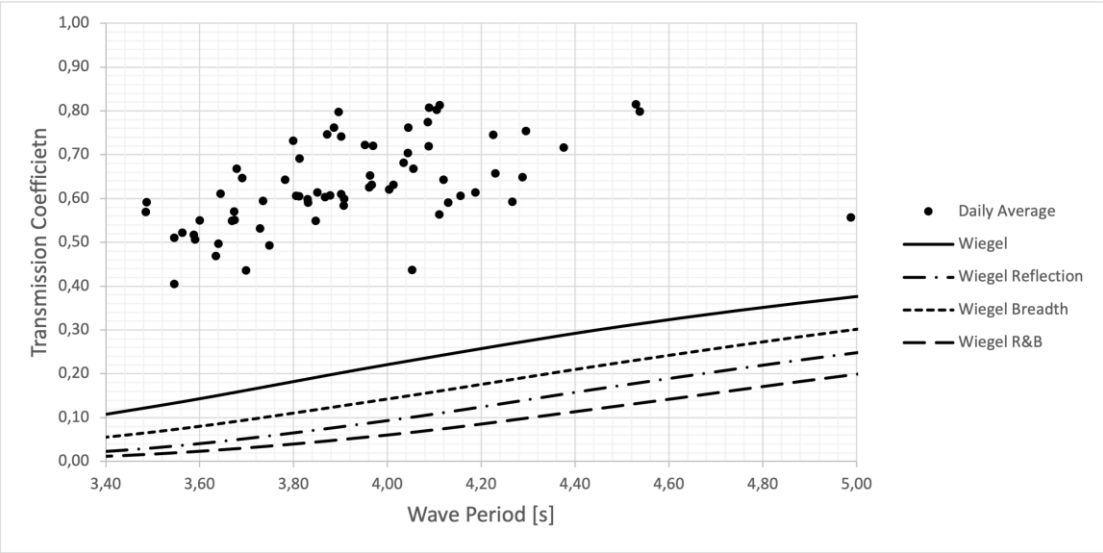

Figure 5.1 Comparison between theoretical Wiegel models and measured transmission at different wave periods.

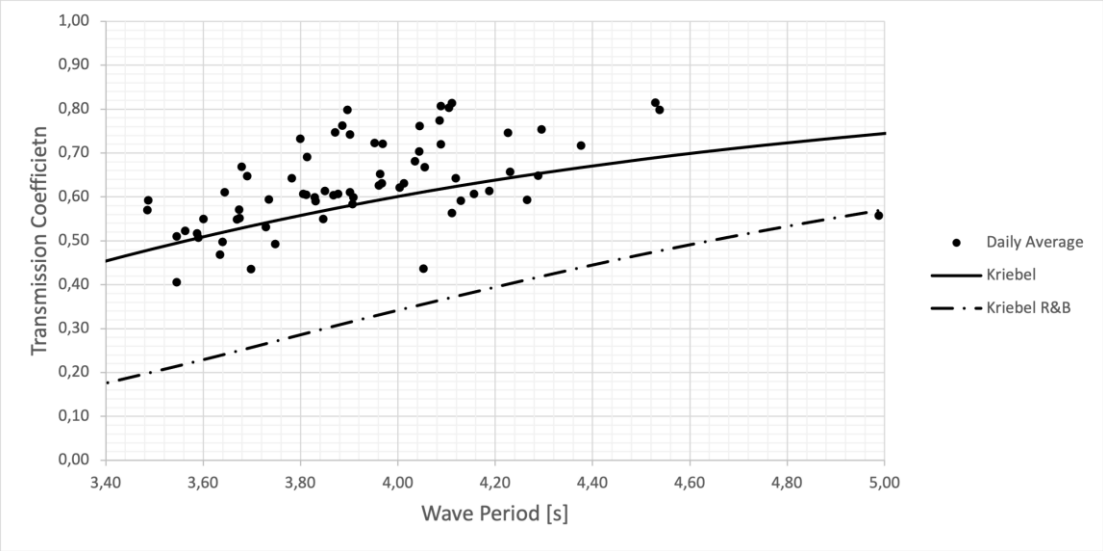

Figure 5.2 Comparison between theoretical Kriebel models and measured transmission at different wave periods.

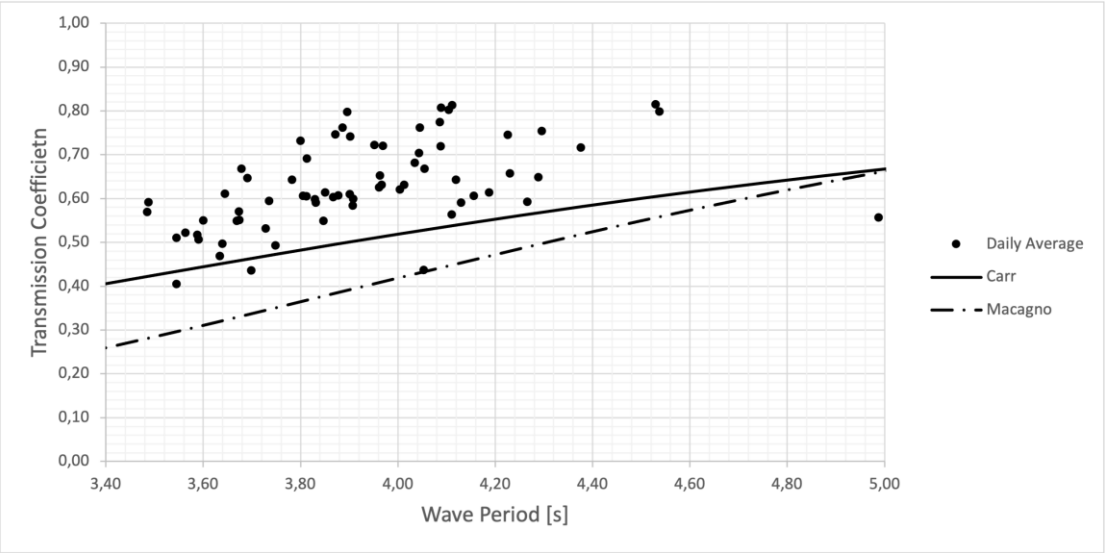

Figure 5.3 Comparison between theoretical models for box-type breakwaters and measured transmission at different wave periods.

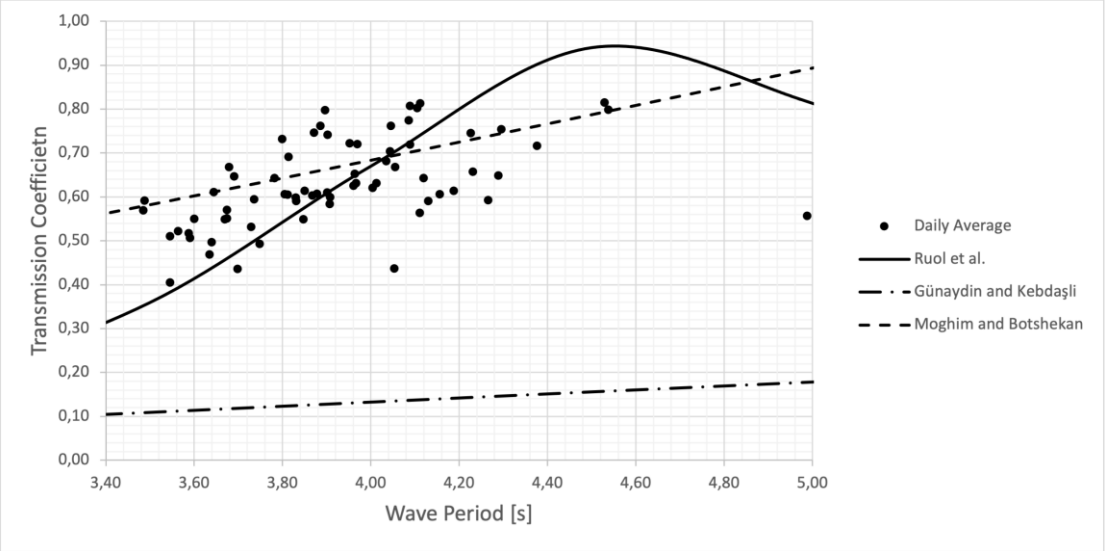

Figure 5.4 Comparison between theoretical models for Π -type breakwaters and measured transmission at different wave periods.

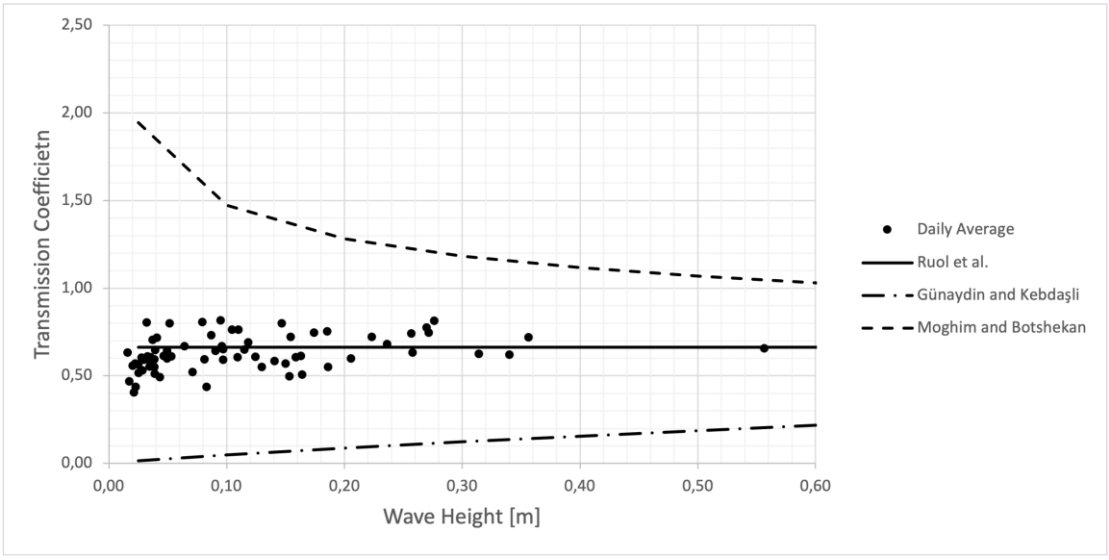

Figure 5.5 Comparison between theoretical models for Π -type breakwaters and measured transmission at different wave heights.

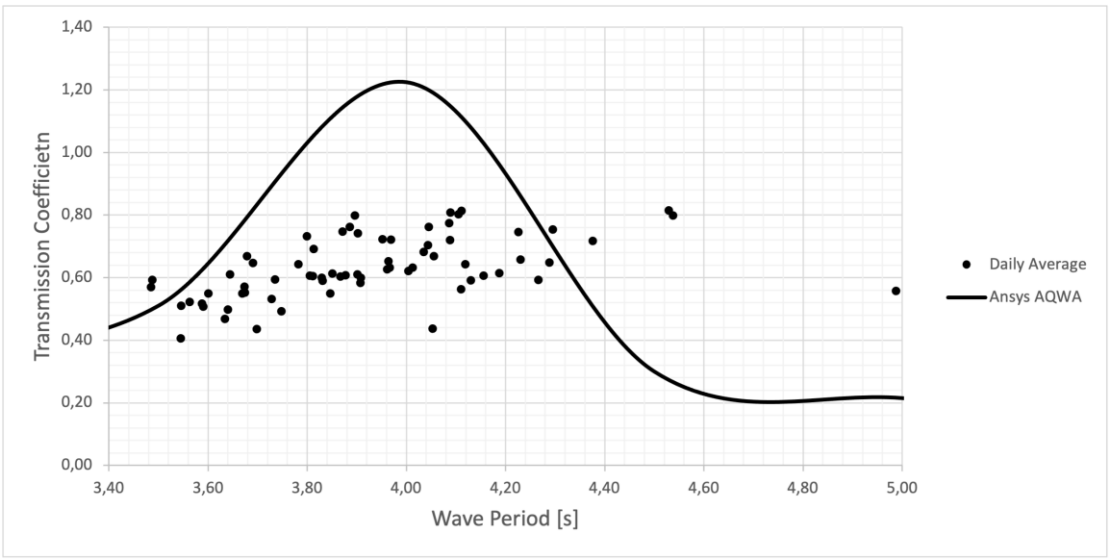

Figure 5.6 Comparison between Ansys AQWA and measured transmission at different wave periods.

5.3 Wave climate and breakwater movement

The movement analysis result presented in Section 4.4, indicates that the roll and pitch movement of the breakwater are dependent on the wave climate. Analyzing Figure 4.36 and Figure 4.37 shows that the maximum obtained roll and pitch angle increases with an increased incoming significant wave height.

Figure 4.38 and Figure 4.39 indicate a peak angle at a wave period of around 4 seconds and an overall increasing angle with an increasing wave period. This is expected since the wavelength increases with an increased period and in turn, the relation between the wavelength and breakwater width decreases. With longer waves, the breakwater will move up and down slowly with the wave.

The peak of roll and pitch angles at 4 seconds could have something to do with the natural roll and pitch frequency of the breakwater. In Section 4.4.2 the natural roll frequency was calculated to be 2.33 seconds and the natural pitch frequency was calculated to be 2.06 seconds. Since these values do not take into account the anchoring and connections between breakwaters, natural frequencies could likely have something to do with the peaks at 4 seconds. To verify this, a proper analysis of the natural frequencies of the breakwater, including anchoring and connections, needs to be conducted.

As discussed at the end of Section 4.4.1 there seems to be some relation between the breakwater movement and the transmission performance of the breakwater. Due to the low amount of data points, it is not possible to draw any accurate conclusions regarding how this relation looks. If the wave recorder on the inside would have been obtained after the last measurement a better analysis of this relation would have been possible.

5.4 Development of a new model

In Section 1.2 it was mentioned that a new model should be developed using the results of this study. To develop a model, more measurements need to be conducted where the properties of the breakwater and location change. The measurements that have been carried out have been on one breakwater, with one anchoring system, at one location. Due to this, the results do not show how a change of the width, draft, water depth, or any other property, changes the transmission of the breakwater.

6 References

Adafruit (2021, 3 Mars). *Adafruit Dara Logger Shield, Overview*. https://learn.adafruit.com/adafruit-data-logger-shield

Airy, G. B. (1845). Tides and waves. *Encyc. Metrop.*, Article 192, 1845, pp. 241-396.

Akhemka. (2020). *How to output Ansys AQWA pressure contour as .CSV file?* Ansys Learning Forum. https://forum.ansys.com/discussion/22539/how-to-output-ansys-aqwa-pressure-contour-as-csv-file

Arduino (n.d.) *Arduino Uno Rev3 SMD*. https://store.arduino.cc/arduino-uno-rev3-smd

Ansys (2012). *AQWA User Manual* [Fact sheet]. https://cybership.files.wordpress.com/2014/01/wb_aqwa.pdf

Carr, J. H. (1951). Mobile Breakwaters. *Coastal Engineering Proceedings*, 1(2), 25. https://doi.org/10.9753/icce.v2.25

Cederwall, K., Larsen, P. (1979). *Hydraulik för väg- och vattenbyggare* [Hydraulics for civil engineers]. LiberLäromedel.

Coastal Engineering Research Center (US). (1984). *Shore Protection Manual, Volume 1*. (4th ed.) Department of the Army, Waterways Experiment Station, Corps of Engineers, Coastal Engineering Research Center.

Cox, R., Beach, D. (2006). Floating breakwater performance – Wave transmission and reflection, energy dissipation, motions and restraining forces. *In Proceedings of the first international conference on the application of physical modelling to port and coastal protection*, pp. 371-381.

Dai, J., Wang, C. M., Utsunomiya, T., Duan, W. (2018). Review of recent research and developments on floating breakwaters. *Ocean Engineering*, Vol. 158, June 2018, pp. 132-151. https://doi.org/10.1016/j.oceaneng.2018.03.083

ELJI electronics (n.d.). *Klimatdata för Säby, Tjörns kommun*. https://elji.se/index.php/klimatdata/

Faltinsen, O. M. (1990). *Sea Loads on ships and offshore structures.* Cambridge University Press, Cambridge, United-Kingdom.

Folley M. (2017). *The Wave Energy Resource*. In: Pecher A., Kofoed J. (eds) Handbook of Ocean Wave Energy. Ocean Engineering & Oceanography, Vol 7. Springer, Cham. https://doi.org/10.1007/978-3-319-39889-1_3

Goodknight, R.C., Russel, T.L. (1963). Investigation of the statistics of wave heights. *Journal of the Waterways and Harbours Division*. Vol. 89, No. 2, May 1963. https://doi.org/10.1061/JWHEAU.0000325

Günaydin, K., Kabdaşli, M.S. (2007). Investigation of Π-type breakwaters performance under regular and irregular waves. *Ocean Engineering*. Vol. 34, No. 7, May 2007, pp. 1028-1043. https://doi.org/10.1016/j.oceaneng.2006.03.015

Hunt, J.N. (1979). Direct solution of wave dispersion equation. *Journal of Waterway, Port, Coastal and Ocean Division*, Vol. 105, No. 4, November 1979, pp. 457-459.

Institution of Civil Engineers (1992). *Coastal Structures and Breakwaters: Proceedings of the Conference Organized by the Institution of Civil Engineers, and Held in London on 6-8 November 1971*. Thomas Telford, London, Great Britain.

Janson, C.-E. (2015). *Waves, Motions and Manoeuvring: Lecture Notes for SJO745 Wave loads and seakeeping*. Department of Shipping and Marine technology. Gothenburg: Chalmers University of Technology.

Kamphuis, J. W. (2000). *Introduction to Coastal Engineering and Management*, World Scientific, Singapore.

Kriebel, D. L., Bollmann, C. A. (1996, 2-6 September). Wave transmission past vertical wave barriers. *25th International Conference on Coastal Engineering*, Orlando, Florida, United States. https://doi.org/10.1061/9780784402429.191

Kriebel, D. L. (2000). Performance of vertical wave barriers in random seas. *Proc., Coastal Structures' 99*, Rotterdam, The Netherlands: Balkema. pp. 525-532.

Le Roux, J. P. (2007). A function to determine wavelength from deep into shallow water based on the length of the cnoidal wave at breaking, *Coastal Engineering*, Vol. 54, No. 10, October 2007, pp.770-774. https://doi.org/10.1016/j.coastaleng.2007.05.004

Macagno, E. O. (1953). Mécanique des fluids - sur les effects de passages des houles planes sous un obstacle [Fluid mechanics Experimental study of the effects of the Passage of a wave beneath an obstacle]. *Proceedings of the Academic des Sciences*, Paris, France.

MarCom Working Group (1995). *Criteria for movements of moored ships in harbours, a practical guide*. PIANC.

MATLAB (2018, December 12). *Sensor Fusion for Orientation Estimation* [Video]. YouTube. https://www.youtube.com/watch?v=UZsxFpjmdAs&t=946s

McCartney, B. (1985). Floating breakwater design. *Journal of waterway, port coastal and ocean engineering*, Vol. 111, No. 2, pp. 304-318.

Moghim, M. N., Botshekan, M. (2017). Analysis of the performance of pontoon-type floating breakwaters. *HKIE Transactions*. Vol. 24, No. 1, Mars 2017, pp. 9-16. http://dx.doi.org/10.1080/1023697X.2016.1262292

Peña González, E., Sánchez-Tembleque Díax-Pache, F., López Merino, A., Costa González, F., Fernández López, T., Ferras Robles, J. (2011). *Transmission coefficient model scale study of the SF600 Marine System International floating breakwater*. University of A Coruña, Spain.

Ruol, P., Martinelli, L., Pezzutto, P. (2013). Formula to predict transmission for π-type floating breakwaters. *Journal of Waterway, Port, Coastal, and Ocean Engineering*, Vol. 139, No. 1, January 2013. https://doi.org/10.1061/(ASCE)WW.1943-5460.0000153

Sadeghi, K. (2008). Significant Guidance for Design and Construction of Marine and Offshore Structures. *GAU Journal of Social & Applied Sciences,* Vol. 4, No. 7, 65 – 92.

SMHI (n.d.). *Ladda ner meterologiska observationer, Måseskär A* [Download meteorological observations, Måseskär A] https://www.smhi.se/data/meteorologi/ladda-ner-meteorologiska-observationer/#param=wind,stations=all,stationid=81050

SMHI (n.d.). *Ladda ner oceanografiska observationer*. [Download oceanographic observations]]https://www.smhi.se/data/oceanografi/ladda-ner-oceanografiska-observationer#param=seatemperature,stations=all

Sparkfun (2015). *LSM9DS1 Breakout Hookup Guide*. https://learn.sparkfun.com/tutorials/lsm9ds1-breakout-hookup-guide/all

Thomson, R. E., Emery, W. J. (2014). Chapter 6: Digital filters. In *Data Analysis Methods in Physical Oceanography* (Third Edition) (pp. 593-637). Elsevier. https://doi.org/10.1016/B978-0-12-387782-6.00006-5

Tsinker, G. P. (1995). *Marine structures engineering: Specialized Applications*, Springer Science + Business Media, Boston, United States, https://doi.org/10.1007/978-1-4615-2081-8

Ursell, F. (1947). The effect of a fixed vertical barrier on surface waves in deep water. *Mathematical Proceedings of the Cambridge Philosophical Society*, Vol. 43, No. 3, July 1947, pp. 374-382. https://doi.org/10.1017/S0305004100023604

Valeport Limited. (2008). *MIDAS DWR & WTR Wave Recorders Operation Manual* [Fact sheet]. https://www.valeport.co.uk/content/uploads/2020/03/Midas-DWR-Operating-Manual-0730890b.pdf

Wiegel, R. L. (1960). Transmission of waves past a rigid vertical thin barrier. *Journal of the Waterways and harbour division*, Vol. 86, No. WW1, March 1960, pp. 1-12.

Wiegel, R. L. (1992). *Oceanographical Engineering*. Dover Publications, Mineola, New York, United States

Appendix A

Measured probability of different wave climates.

Probability	Wave Period																			Total
Significant Wave Height	2,0	2,5	3,0	3,5	4,0	4,5	5,0	5,5	6,0	6,5	7,0	7,5	8,0	8,5	9,0	9,5	10,0	
0,00	0,00%	0,02%	2,39%	15,98%	10,81%	7,66%	2,02%	0,22%	0,04%	0,00%	0,00%	0,00%	0,08%	0,06%	0,08%	0,06%	0,00%	39,4%
0,10	0,00%	0,00%	0,76%	13,18%	9,71%	7,19%	1,68%	0,16%	0,02%	0,02%	0,00%	0,00%	0,00%	0,00%	0,00%	0,00%	0,00%	32,7%
0,20	0,00%	0,00%	0,25%	5,44%	5,19%	3,78%	0,33%	0,00%	0,00%	0,00%	0,00%	0,00%	0,00%	0,00%	0,00%	0,00%	0,00%	15,0%
0,30	0,00%	0,00%	0,04%	1,76%	2,55%	2,45%	0,43%	0,00%	0,00%	0,00%	0,00%	0,00%	0,00%	0,00%	0,00%	0,00%	0,00%	7,2%
0,40	0,00%	0,00%	0,02%	1,06%	1,18%	0,86%	0,37%	0,02%	0,00%	0,00%	0,00%	0,00%	0,00%	0,00%	0,00%	0,00%	0,00%	3,5%
0,50	0,00%	0,00%	0,00%	0,29%	0,39%	0,33%	0,16%	0,04%	0,00%	0,00%	0,00%	0,00%	0,00%	0,00%	0,00%	0,00%	0,00%	1,2%
0,60	0,00%	0,00%	0,00%	0,18%	0,16%	0,12%	0,10%	0,02%	0,02%	0,00%	0,00%	0,00%	0,00%	0,00%	0,00%	0,00%	0,00%	0,6%
0,70	0,00%	0,00%	0,00%	0,04%	0,06%	0,06%	0,00%	0,00%	0,02%	0,00%	0,00%	0,00%	0,00%	0,00%	0,00%	0,00%	0,00%	0,2%
0,80	0,00%	0,00%	0,00%	0,00%	0,08%	0,02%	0,00%	0,00%	0,00%	0,00%	0,00%	0,00%	0,00%	0,00%	0,00%	0,00%	0,00%	0,1%
0,90	0,00%	0,00%	0,00%	0,02%	0,00%	0,00%	0,00%	0,00%	0,00%	0,00%	0,00%	0,00%	0,00%	0,00%	0,00%	0,00%	0,00%	0,0%
1,00	0,00%	0,00%	0,00%	0,00%	0,00%	0,00%	0,02%	0,00%	0,00%	0,00%	0,00%	0,00%	0,00%	0,00%	0,00%	0,00%	0,00%	0,0%
1,10	0,00%	0,00%	0,00%	0,02%	0,00%	0,00%	0,00%	0,00%	0,00%	0,00%	0,00%	0,00%	0,00%	0,00%	0,00%	0,00%	0,00%	0,0%
1,20	0,00%	0,00%	0,00%	0,00%	0,00%	0,00%	0,00%	0,00%	0,00%	0,00%	0,00%	0,00%	0,00%	0,00%	0,00%	0,00%	0,00%	0,0%
Total	0,0%	0,0%	3,5%	38,0%	30,1%	22,5%	5,1%	0,5%	0,1%	0,0%	0,0%	0,0%	0,1%	0,1%	0,1%	0,1%	0,0%	

Appendix B

Calculation of significant and maximum wave height using Weibull distribution.

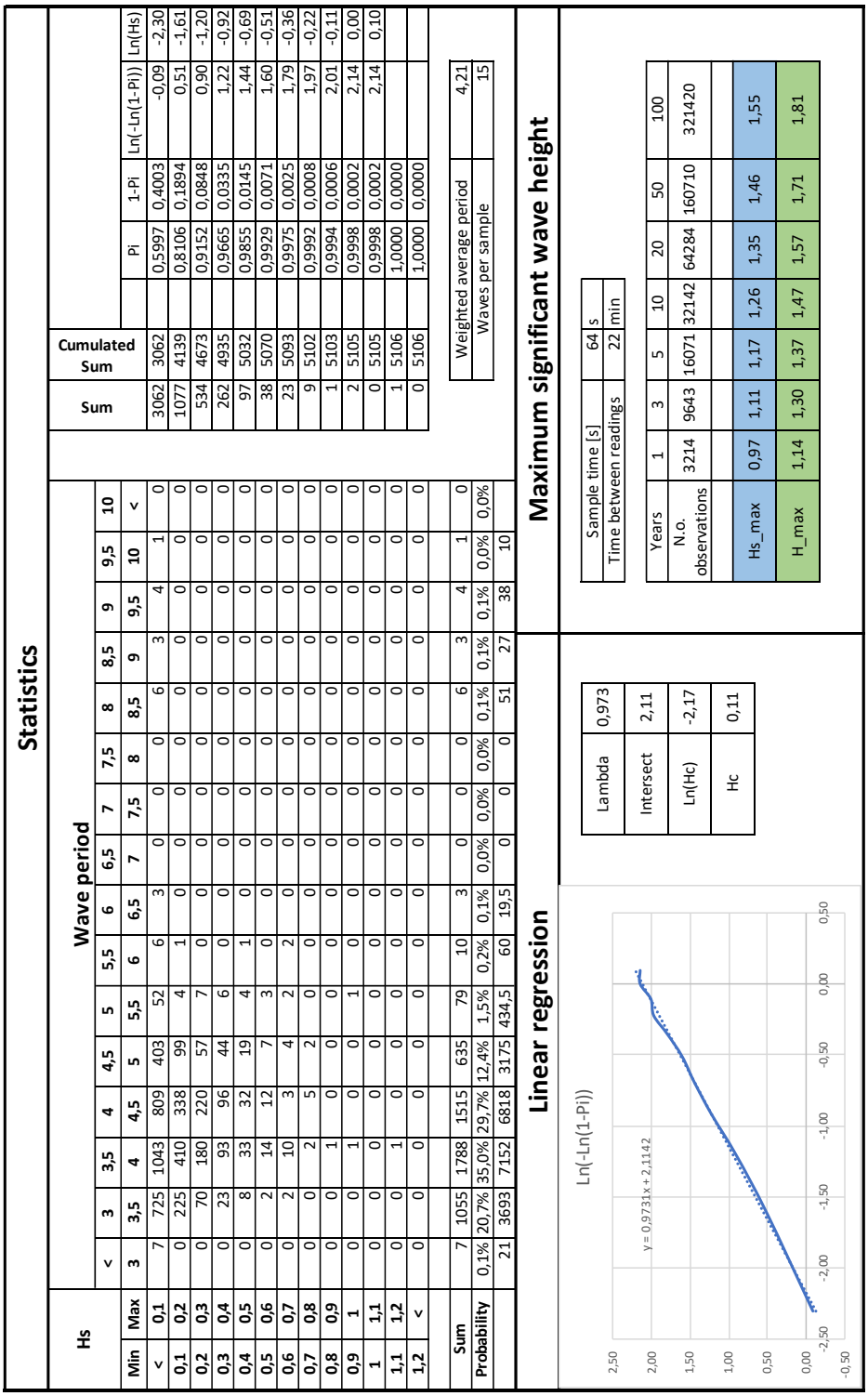

Statistics

Hs		Wave period																	Sum	Cumulated Sum	Pi	1-Pi	Ln(-Ln(1-Pi))	Ln(Hs)
		<	3	3,5	4	4,5	5	5,5	6	6,5	7	7,5	8	8,5	9	9,5	10	<						
Min	Max	3	3,5	4	4,5	5	5,5	6	6,5	7	7,5	8	8,5	9	9,5	10	9,5	10						
<	0,1	7	725	1043	809	403	52	6	3	0	0	0	0	6	3	4	1	0	3062	3062	0,5997	0,4003	-0,09	-2,30
0,1	0,2	0	225	410	338	99	4	1	0	0	0	0	0	0	0	0	0	0	1077	4139	0,8106	0,1894	0,51	-1,61
0,2	0,3	0	70	180	220	57	7	0	0	0	0	0	0	0	0	0	0	0	534	4673	0,9152	0,0848	0,90	-1,20
0,3	0,4	0	23	93	96	44	6	0	0	0	0	0	0	0	0	0	0	0	262	4935	0,9665	0,0335	1,22	-0,92
0,4	0,5	0	8	33	32	19	4	1	0	0	0	0	0	0	0	0	0	0	97	5032	0,9855	0,0145	1,44	-0,69
0,5	0,6	0	2	14	12	7	3	0	0	0	0	0	0	0	0	0	0	0	38	5070	0,9929	0,0071	1,60	-0,51
0,6	0,7	0	2	10	3	4	2	2	0	0	0	0	0	0	0	0	0	0	23	5093	0,9975	0,0025	1,79	-0,36
0,7	0,8	0	0	2	5	2	0	0	0	0	0	0	0	0	0	0	0	0	9	5102	0,9992	0,0008	1,97	-0,22
0,8	0,9	0	0	1	0	0	0	0	0	0	0	0	0	0	0	0	0	0	1	5103	0,9994	0,0006	2,01	-0,11
0,9	1	0	0	1	0	0	1	0	0	0	0	0	0	0	0	0	0	0	2	5105	0,9998	0,0002	2,14	0,00
1	1,1	0	0	0	0	0	0	0	0	0	0	0	0	0	0	0	0	0	0	5105	0,9998	0,0002	2,14	0,10
1,1	1,2	0	0	1	0	0	0	0	0	0	0	0	0	0	0	0	0	0	1	5106	1,0000	0,0000		
1,2	<	0	0	0	0	0	0	0	0	0	0	0	0	0	0	0	0	0	0	5106	1,0000	0,0000		
Sum		7	1055	1788	1515	635	79	10	3	0	0	0	6	3	4	1	0							
Probability		0,1%	20,7%	35,0%	29,7%	12,4%	1,5%	0,2%	0,1%	0,0%	0,0%	0,0%	0,1%	0,1%	0,1%	0,0%	0,0%							
		21	3693	7152	6818	3175	434,5	60	19,5	0	0	0	51	27	38	10								

Weighted average period	4,21
Waves per sample	15

Linear regression

Lambda	0,973
Intersect	2,11
Ln(Hc)	-2,17
Hc	0,11

Maximum significant wave height

Sample time [s]	64	s
Time between readings	22	min

Years	1	3	5	10	20	50	100
N.o. observations	3214	9643	16071	32142	64284	160710	321420
Hs_max	0,97	1,11	1,17	1,26	1,35	1,46	1,55
H_max	1,14	1,30	1,37	1,47	1,57	1,71	1,81

DEPARTMENT OF MECHANICS AND MARITIME SCIENCES
DIVISION OF MARINE TECHNOLOGY
CHALMERS UNIVERSITY OF TECHNOLOGY
Gothenburg, Sweden 2021
www.chalmers.se

CHALMERS
UNIVERSITY OF TECHNOLOGY